GEORGIA INSTITUTE OF TECHNOLOGY OFFICE OF CONTRACT ADMINISTRATION

SPONSORED PROJECT TERMINATION/CLOSEOUT SHEET

2-5A890

Date 5/18/88

Project No. E-16-650 School/~~CEE~~ AE

Includes Subproject No.(s) N/A

Project Director(s) G. A. Flandro GTRC/~~GIT~~

Sponsor McDonnell Douglas Corporation

Title Predicted Spacecraft Attitude Behavior

Effective Completion Date: 8-30-87 (Performance) 8-30-87 (Reports)

Grant/Contract Closeout Actions Remaining:

- [ ] None
- [ ] Final Invoice or Copy of Last Invoice Serving as Final Already submit
- [ ] Release and Assignment (Sponsor sending forms for completion.)
- [x] Final Report of Inventions and/or Subcontract:
  Patent and Subcontract Questionnaire sent to Project Director [x]
- [ ] Govt. Property Inventory & Related Certificate
- [ ] Classified Material Certificate
- [ ] Other

Continues Project No. Continued by Project No.

COPIES TO:

Project Director
Research Administrative Network
Research Property Management
Accounting
Procurement/GTRI Supply Services
Research Security Services
Reports Coordinator (OCA)
Program Administration Division
Contract Support Division
Facilities Management - ERB
Library
GTRC
Project File
Other

CHARACTERISTICS OF NUTATION INSTABILITY IN ULYSSES/PAM-S SPIN STABILIZED SPACECRAFT

submitted to

McDonnell Douglas Astronautics Corporation
5301 Bolsa Avenue
Huntington Beach, CA 92647

by

G. A. Flandro
School of Aerospace Engineering
Georgia Institute of Technology
Atlanta, Georgia 30332
15 September 1987

ABSTRACT

An analysis of the nutation instability characteristics of the PAM-Sorbital injection stage for the Ulysses spacecraft is presented. The spinning upper stage motor is a Thiokol STAR-48 solid propellant rocket, which exhibited nutation instability effects in the earlier PAM-D and SGS-II launch vehicle programs. Wobbling of the spacecraft is apparently induced by interaction between the vehicle motions and either the time-dependent gas flow in the combustion chamber and nozzle or accumlations of aluminum oxide slag in the aft closure of the motor. Rate gyroscope data show that growth of the instability ceases abruptly at motor burnout.

Since the exact nature of the nutation source has not been properly established, estimates of the disturbing torque require application of assumed models for the coning mechanism. In this report the gas dynamic or "jet gain" mechanism based on an Air Force sponsored study is utilized. In this proposed mechanism the nutation disturbance is a closed-loop phenomenon in which the disturbing torque depends on the size, shape, mass flow rate and position of the rocket motor relative to the vehicle mass center. The torque magnitude is independent of vehicle translational acceleration, but depends directly on angular acceleration. If no attitude control system is employed in the Ulysses vehicle, the model predicts that very large wobbling motions will appear near the end of the motor burn mainly as a result of the relatively smaller lateral moments of inertia as compared to PAM-D mass properties. In designing an effective attitude control strategy, body-fixed side forces due to thrust misalignment or center of gravity offsets must be addressed as well as the self-excited jet gain torques. Side forces act as a trigger for the motor induced self-excitation, and the final cone angle and nutation angular rates depend on the side force time history as well as initial conditions at motor ignition.

The Ulysses/PAM-S stage is threatened by possibly intolerable nutation oscillation growth if an active attitude control system is not employed. Since design of an efficient attitude control strategy depends on a detailed knowledge of the nutation mechanism, it is imperative that renewed efforts be made to identify the precise cause of the instability, its dependence on system parameters, and the associated scaling factors. It is recommended that a full-scale testing program using either a compliant spinning static test arrangement or a flight test with motor recovery be used to resolve the mechanism issue. Errors in attitude control system implementation could result if steps are not taken to clarify the nature of the disturbing moment and its relationship to vehicle and motor parameters.

TABLE OF CONTENTS

CHARACTERISTICS OF NUTATION INSTABILITY IN ULYSSES/PAM-S SPIN STABILIZED SPACECRAFT

G. A. Flandro
School of Aerospace Engineering
Georgia Institute of Technology
16 September 1987

1.0 INTRODUCTION

This report describes predicted nutation instability characteristics of the PAM-S spinning payload insertion stage for the Ulysses Solar Probe mission. The predicted coning behavior is based on an updated version of the gasdynamic (*Jet Gain*) instability algorithm described in Air Force Report AFRPL TR 86-072 (Ref. 1). The instability is assumed to result from a closed-loop mechanism involving coupling of a complex, time-dependent motor internal flow with the vehicle dynamics. The model is consistent with experimental data from PAM-D, SGS-II, and PAM-DII flights. Simulated angular motion of the Ulysses vehicle shows aggravated coning behavior due to the relatively smaller moments of inertia compared to PAM-D spacecraft. However, the computations show that the disturbing torque gain factor is approximately the same as that of PAM-D vehicles because the beneficial effect of the shorter moment arm between mass center and the rocket motor is offset by the higher spin rate. It is demonstrated that a simple attitude control system with modest corrective moment capability can prevent self-excited coning instability.

The computations incorporate mass properties and geometry of the PAM-S vehicle. Corrections for effects of unequal lateral moments of inertia are incorporated both in the instability calculations and in the simulations of spacecraft behavior during motor burn. The main goal of the work is the determination of disturbing torques and their relationship to vehicle motions for use in attitude control system design.

For the benefit of readers unfamiliar with the nutation instability phenomenon, a fairly comprehensive background discussion is presented first to emphasize factors pertinent to PAM-S operations. This information should clarify the approach used in estimating the disturbing torques in the PAM-S system. It is followed by a brief discussion of the computational approach and a presentation of the results. Finally, appropriate attitude control strategies based on these findings are recommended.

2.0 THE NUTATION INSTABILITY PROBLEM

The "coning" or "nutation instability" phenomenon has been under study since 1980. This problem was encountered in commercial communication satellite orbit raising operations boosted by Delta and Space Shuttle systems. Residual wobbling motions introduced during deployment and pre-firing coast of the spinning upper stage are enormously amplified during operation of the rocket motor as depicted in Figure 1. The McDonnell Douglas PAM-D and PAM-DII vehicles all using variants of the Thiokol STAR 48 and IPSM motor technology have experienced this phenomenon. Table 1 summarizes the experimental evidence. Wobbling amplitudes at motor burnout as measured by the final cone angle as shown in Figure 1 have averaged about 10 degrees and have reached values as high as 17 degrees.

Large nutation divergence was successfully avoided in the Air Force SGS-II satellite launches by means of a strap-on nutation control system (NCS). There was concern that the compounding of the coning effects in the two-stage (two spinning STAR-48 motors) would seriously degrade the mission objectives. The design of the NCS for these launches was relatively straightforward since the second stage (carrying the payload package) had mass properties similar to the earlier PAM-D vehicles; the more massive first STAR-48 stage was expected to be less sensitive to disturbing torques. It was therefore possible to use a disturbance model based on the PAM flight data. This procedure is likely inappropriate in designing nutation control systems for vehicles with mass properties significantly different than those of the PAM-D, especially if lateral moments of inertia are substantially smaller. It is necessary to know the origins and characteristics of the disturbing mechanism in detail to design an effective and reliable NCS system.

The disturbing source is clearly related to operation of the rocket motor; growth of the wobbling amplitude ceases abruptly at the end of burn. The final dropoff in the growth rate closely follows the combustion gas mass flow rate decrease during the taildown process. However, the exact mechanism by which the motor can generate the unbalanced side forces or moments that drive the wobbling motion has been very difficult to isolate. Side forces due to thrust misalignment have been measured in static (spinning) motor tests, but although these couple with the vehicle nutation, it is readily demonstrated that they cannot be the primary cause of the instability. The disturbing torque must move relative to the vehicles, and it must be synchronized with the natural wobbling oscillations in a specific way.

Soon after flight data from the first PAM-D vehicles were analyzed showing the presence of an unexpected attitude stability problem, an intensive effort was initiated by several agencies to determine the cause of the difficulty. These attempts focused mainly

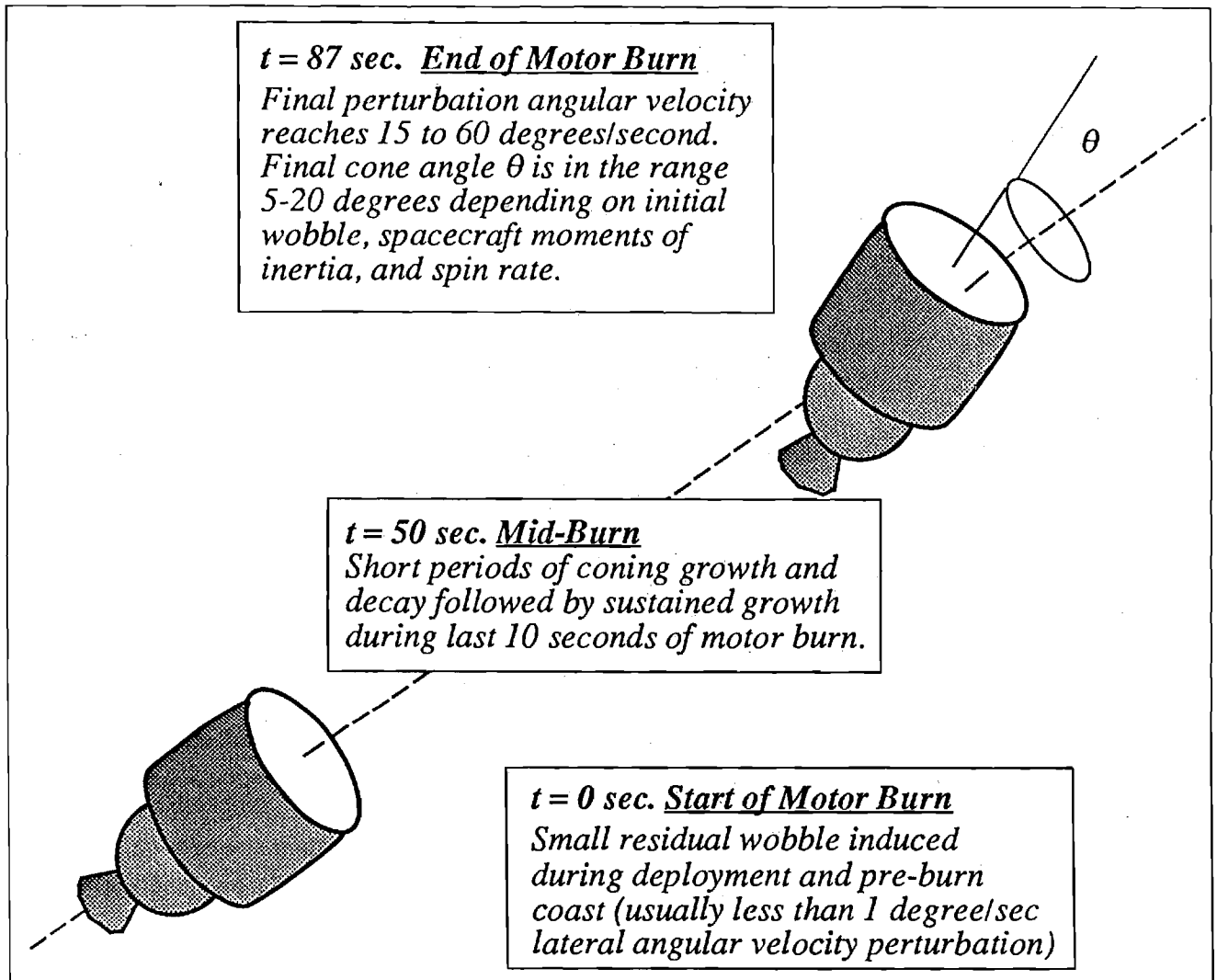

Figure 1. Development of Coning Instability During Motor Burn (PAM-D, STAR 48)

on well-known spinning body instability mechanisms. A mechanism based on vibration of the relatively large and flexible nozzle exit cone of the STAR 48 motor was tested in flight and proved not to be the cause of the instability. Several later studies attempted to establish slag accumulation within the motor as the source of the perturbing torques. However, experimental simulation of slag dynamic effects by McDonnell Douglas indicated that either unrealistic amounts of slag or unjustifiable assumptions concerning the geometry and motion of the slag pool were required to match flight data.

Failure of the nozzle modifications to eliminate coning led to an intensive Air Force (AFAL) sponsored study[1]. Research was aimed at clarifying the potential role of the internal gas dynamics of the rocket motor in the coning phenomenon. This was an area not considered by McDonnell Douglas and by the Aerospace Corporation in their earlier

studies of the problem. The Air Force study indicated that internal ballistics of the motor must be regarded as a possible source of the instability. There is considerable evidence that the gas dynamic interactions (to be referred to herein as the "jet gain"effect because of its relationship to the classical "jet damping" effect) closely fit the experimental evidence. The jet gain is the time-dependent analog of the steady flow jet damping.

Results from all previous studies, and in particular the findings of Reference 1, show that a parameter of major importance in the final coning angle for space vehicles of the PAM-D class is the lateral centroidal moment of inertia, I_1. The growth rate of the coning disturbance depends inversely on I_1. Since the moments of inertia decrease rapidly as propellant is consumed, the final coning amplitude depends in a complicated way on this parameter. Figure 2 shows the sensitivity of the final cone angle to the lateral moment of inertia. The abscissa is the ratio of the I_1 to a value characteristic of the PAM-D vehicles. A standard value of $I_{std} = 630$ slug ft^2 was assumed, which is typical of the final moment of inertia of the PAM-D data set shown in Table 1. Thus the final moment of inertia ratio,

$$n = \frac{I_1}{I_{std}} \tag{1}$$

is a useful parameter as plotted in Figure 2 against the resulting final cone angle. All of the measured data closely follow the theoretical results from Reference 1 as shown by the solid curve. This is compelling evidence in support of the gas dynamic mechanism identified in the earlier Air Force work. Actual data from the PAM data set are superimposed for comparison to the theory as represented by the solid line. The four SGS first stage vehicles appear (as a single point) at the extreme right of the plot. Coning data were available for these stages because the deadband of the nutation control system was set higher (2 degrees per second) than the actual rate produced. In SGS flight number 2, a disturbance of unknown origin during the pre-ignition coast phase led to an initial lateral angular rate of about 1.4 degrees per second, which generated a nutation response just within the deadband. The time-history of this response was similar in most respects to the PAM-D data with a final pitch angular velocity just under 2 degrees per second. The low coning response results from the large moment of inertia of the first stage. The second (upper) stage SGS vehicles with lateral moments of inertia similar to that of the PAM-D were successfully controlled by action of the NCS (nutation control system) which limited the wobbling to less than the deadband value.

Of great practical importance is the increasing sensitivity of the final cone angle to the lateral moment of inertia for values of n less than unity. This indicates that for payloads lighter than the PAM-D vehicles using the STAR-48 propulsion system, greatly increased final cone angles are possible. The theory indicates that for a vehicle with a final lateral moment of inertia approximately half that of the standard PAM value, the cone

angle approaches the 90 degree maximum theoretical value. Since the Ulysses configuration has a value of n of approximately 0.6, there is obviously cause for concern as indicated in Figure 2. Figure 3 shows the moment of inertia time histories for the Ulysses vehicle assumed in the stability calculations to be discussed later. The data points in the plots correspond to polynomial fits used to represent the spacecraft parameters in the computational algorithms.

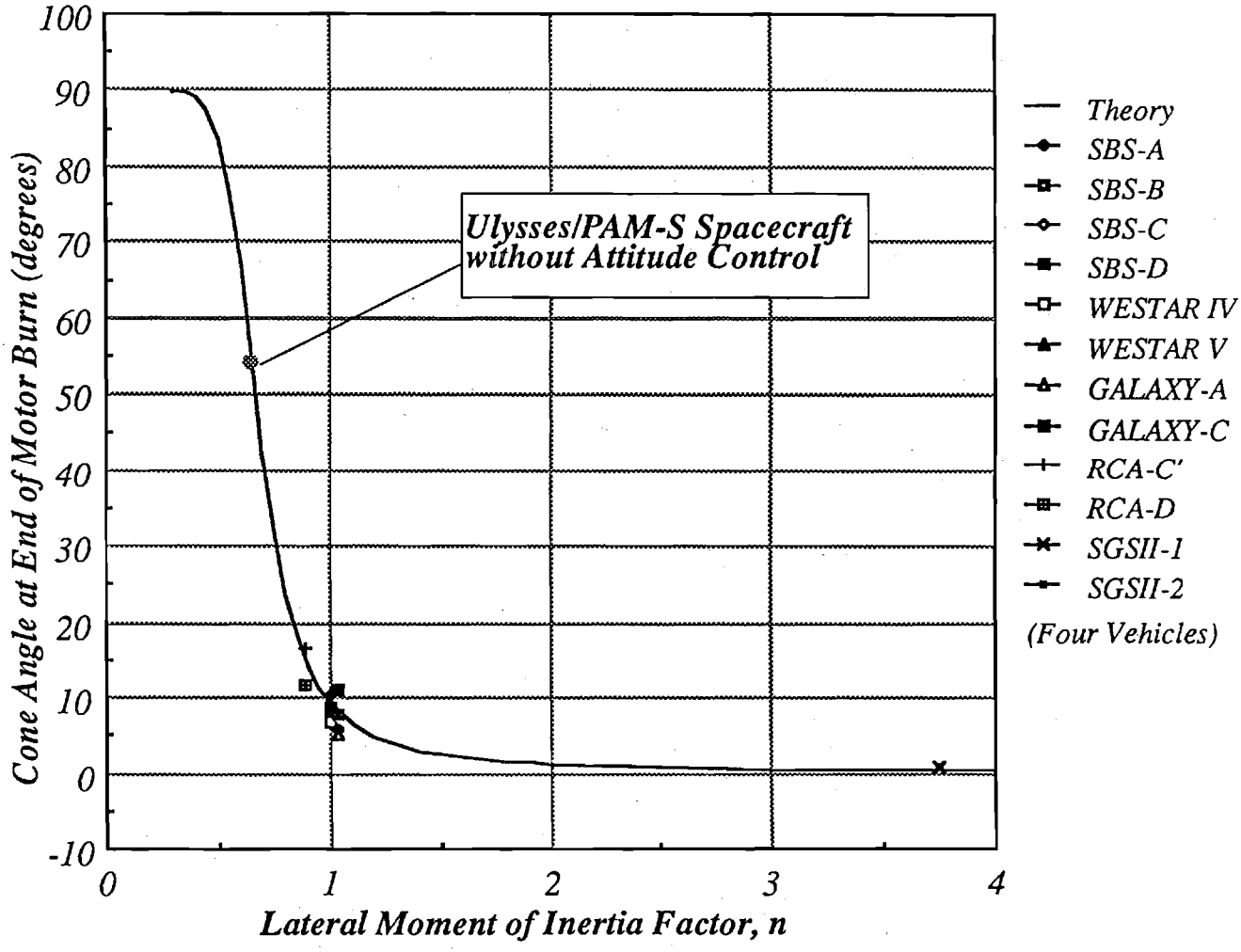

Figure 2. Effect of Lateral Moment of Inertia on Coning Growth

Some investigators have suggested that, since the data indicate the propulsion system is the primary cause of the instability, use of a different solid propellant motor could eliminate the risk. However, the jet gain model indicates that any solid propellant space motor in the performance range and burning time range of the STAR 48 is likely to exhibit coning instability. The fact that the phenomenon had not been observed before the advent of the PAM series was shown in Reference1 to result mainly from the relatively larger motor size needed for orbit raising operations. This is verified by data from the two PAM-DII flights made before cessation of Space Shuttle operations. These vehicles used a larger motor (63 inch diameter as compared to 48 inches for the STAR 48 motors) based

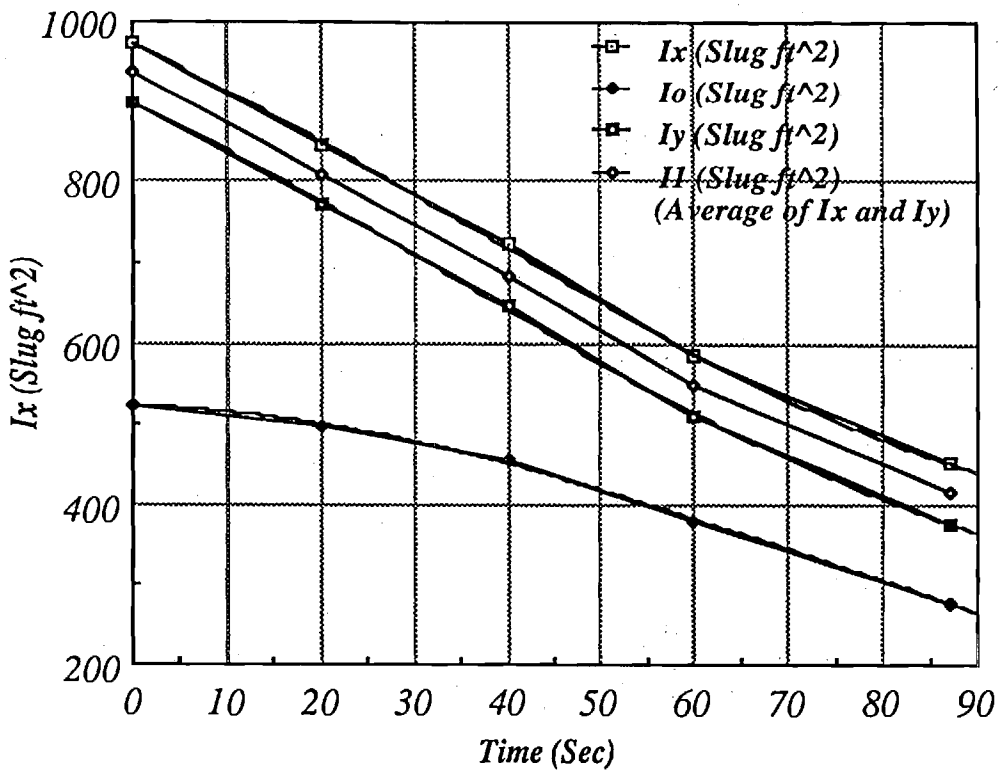

Figure3. Ulysses Moments of Inertia vs Time

on the IPSM technology with a burning time of about 120 seconds. Final cone angles of approximately 13 degrees were observed although the payloads were considerably more massive (final I_1 for the two RCA KuBand vehicles was twice that of the standard value for the PAM-D, about 1260 slug ft^2).

Figure 4 compares the theoretical final cone angle sensitivities for the PAM-D and DII vehicles. The relatively larger values for the DII result from the considerably larger motor size and longer burning time. The curve indicates that if a DII motor were to be used to boost a PAM-D sized payload, the final cone angle would approach the 90 degree limiting value.

Figure 5 presents estimated propulsive impulse loss as a function of final cone angle. Clearly, as the thrust vector deviates from the flight direction during the coning growth during the final 10-20 seconds of motor burn, a sizable performance loss can result from the increasingly helical flight path. The performance loss is not a serious concern for vehicles of the PAM-D class, but a final cone angle of 50 degrees would represent about a 7% loss of impulse. Considering the large expenditure of resources devoted by motor producers to increasing propellant and motor performance by values of this order of magnitude, it is clear that avoidance of nutation instability is absolutely necessary.

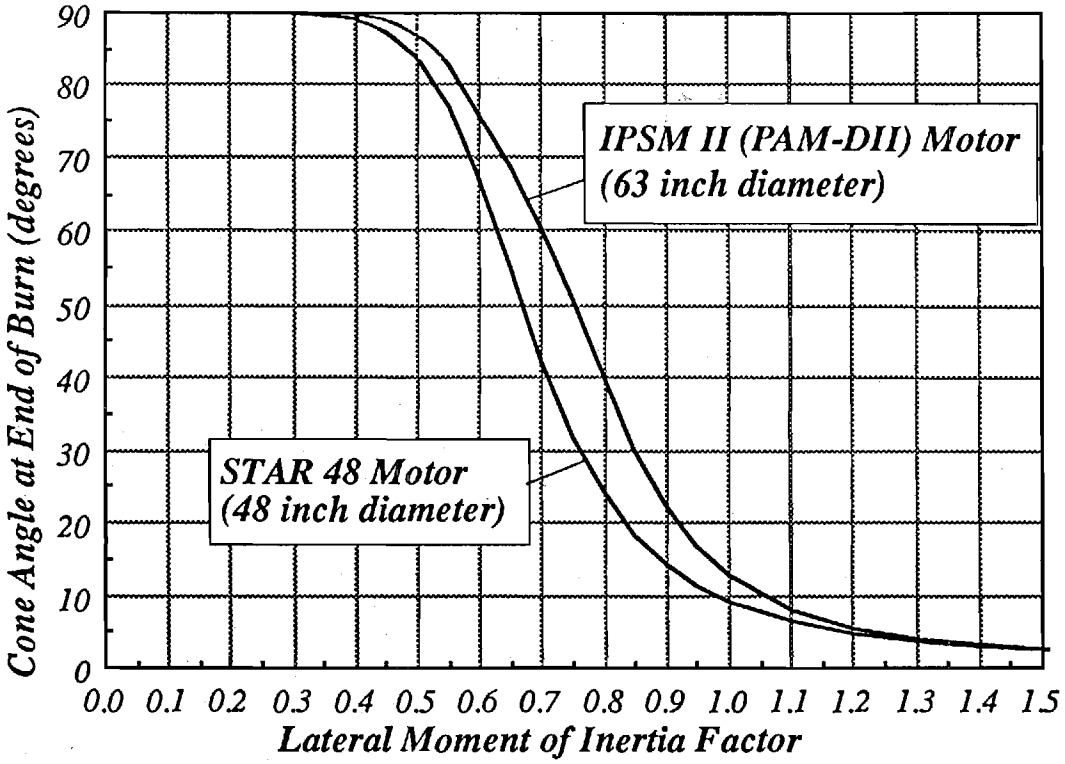

Figure 4. Effect of Motor Size on Final Cone Angle

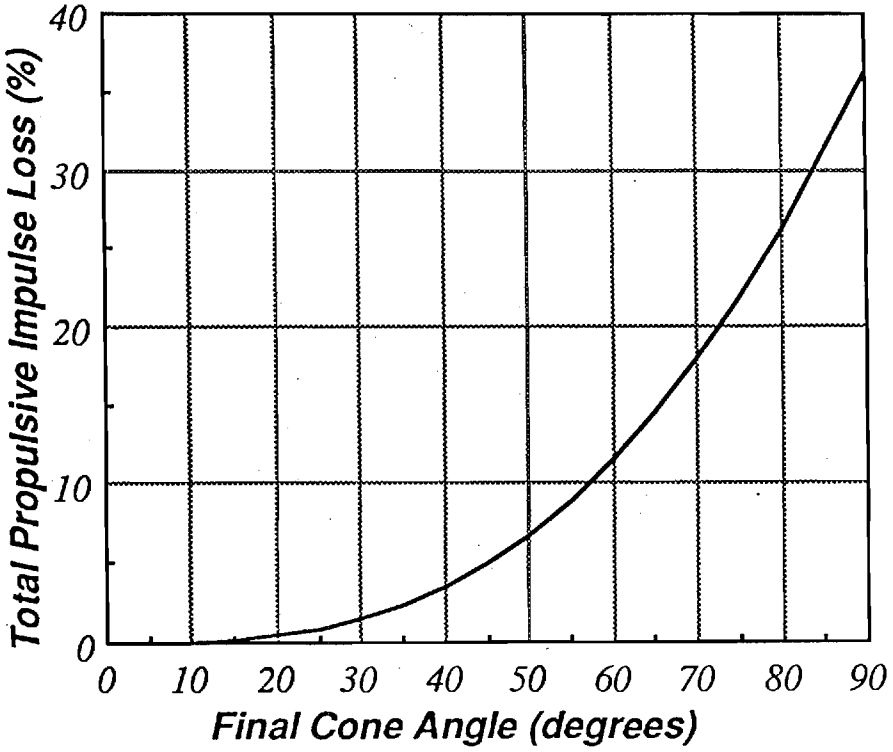

Figure 5. Propulsive Loss due to Nutation Instability

Possible Nutation Driving Mechanisms

Early attempts to explain the instability were based on misalignment or unbalance of the spacecraft or on flexing of structural elements. The former was motivated by the thrust line offsets often observed in solid rockets. The latter is the best-known source of spacecraft wobbling. For example, the tumbling of the first U.S. satellite, the Explorer I, was caused by energy dissipation in its flexible whip antennas. Explorer XX underwent rapid spin decay as a result of Solar torques on a thermally deformed structure. The ATS 5 became unstable as the result of energy dissipation in a heat pipe despite the fact that it was equipped with an active nutation damper during orbital injection.

The appearance of the nutation instability phenomenon in the early flights of the STAR 48 propelled PAM-D (Payload Assist Module-Delta), represented a distinct surprise to the analysts. No similar behavior had been observed in over a decade of experience with spinning solid propellant upper stages. Tumbling of prolate objects spinning about the axis of symmetry is a well-known phenomenon, but the appearance of a rather large instability during the motor burn was unexpected. This was due to the expectation that jet damping would dissipate any residual wobble remaining at motor ignition or induced by thrust offsets during ignition or taildown transients.

A series of very similar spinning vehicles using the smaller STAR 37 motor did not exhibit coning. Data from these flights are included in Table 1 for comparison to the PAM observations. It is noteworthy that the STAR 37 burning period is only about half that of the STAR 48 and a third that of the larger PAM-DII motor. Length of burn (and corresponding relatively larger size of the rocket motor) is the only major apparent difference between earlier vehicles and the STAR 48 PAMs.

It is important to understand that there has been great variability in the configurations of the PAM vehicles in terms of mass properties (mass, moments of inertia, moment arms, etc.) and the details of the payload. While it is possible that flexing structural members, loose deployables, or thermally induced distortion could play some role in the PAM problem, such mechanisms are not compatible with its nearly reproducible nature. The only vehicle element that remained virtually unchanged was the propulsion system itself. Minor changes in nozzle geometry appear to have no large effect on the nutation behavior. A mechanism that was once thought to be the most likely source of the nutation disturbance was vibrational flexing of the nozzle exit cone. However, a flight test (WESTAR V) employing a specially stiffened nozzle failed to exhibit any significant change in the characteristics of the instability.

Sloshing of liquid stores was considered as another possible disturbing entity. There is clear evidence of sloshing effects in the vehicles that carried such materials in the form of continued coning growth (at a substantially reduced rate) after motor burnout.

However, many PAM payloads did not carry liquids or loose parts. Therefore effects of liquid stores cannot be the cause of the pronounced growth during the motor burn. Past experience with sloshing led some investigators to suspect that sloshing of aluminum oxide slag, which accumulates in the motor during combustion, could account for the disturbing torque. However, several years of work by many investigators have failed to yield convincing evidence that this is the primary source of the PAM problem. Study of this mechanism continues at the time of writing. As with the gas dynamic mechanism to be described next, what is required is unambiguous experimental verification. Investigators are devising free-flight tests of small-scale simulated spinning rockets to provide such verification. The status of the experiments is not known at this time, but previous work at McDonnell Douglas using an elaborate laboratory simulation indicated that slag accumulation was an unlikely source of the disturbing torques.

On the basis of careful consideration of the spacecraft observations, it has been apparent to some investigators that the flow of gases through the combustion chamber and the nozzle might represent a significant influence on the nutation. The earliest suggestions of this type were described in an internal NASA document by Bolster[2] with an attachment written by J. F. McGarvey[3]. McGarvey realized that wobbling of the spinning vehicle would be transmitted into the relative gas flow, and he hypothesized a mechanism involving an unsymmetrical pressure distribution within the recirculation region aft of the submerged nozzle entrance. These documents were passed to W. Andrepont at AFRPL who, because of his experience with time-dependent rocket motor flow, recognized the validity of the general concept that the combustion gas flow could be involved. His insight led eventually to the Air Force sponsored study[1] that forms the basis for the present application to the Ulysses orbit insertion propulsion system.

It has now become apparent that the coning instability is not the result of a flaw in the design of the spinning solid propellant motor. The results of the Air Force sponsored study presented in Reference 1 make it clear that a possible cause of the instability is a natural phenomenon involving the response of the combustion gas flow to the lateral movement of the spacecraft. The unbalanced disturbing moment produced in this manner is the direct, unsteady analog of the classical jet damping effect. Jet damping accounts only for the steady part of the internal flow field. Previous jet damping calculations have not accounted for either the time-dependent response of the flow or the axial vortex flow generated within the motor by vehicle spin. It is important to note that the jet damping moment is of the same order of magnitude as the torque that drives the coning motion (but of opposite sign). Also, the time history of the jet damping is similar to the disturbing torque although it always acts to damp lateral oscillations.

A major element of the phenomenon is the strong axial vortex core produced within the nozzle by the vehicle spin. The circumferential flow velocity induced by the vortex velocity field is greately intensified as the vortex core is "stretched" through the nozzle

throat. Small wobbling (nutation) of the spacecraft induces an unsymmetrical pressure pattern within the combustion chamber that is related to the classical inertial wave phenomenon. The fluctuating velocity field associated with this wave interacts strongly with the vortex core, and the resulting unsteady gas motion is an undulating vortex filament orbiting the chamber axis as it leaves through the nozzle. Figure 6 illustrates in a simplified form the flow field in the nozzle entrance. The origin of an unbalanced side force is clearly in evidence.

From a control volume viewpoint, the result of the flow described in the last paragraph is a net outflow of lateral angular momentum. This angular momentum flux is accompanied by a torque acting on the spacecraft that can exceed the jet damping moment. This is not a large torque. For the PAM vehicles its maximum value is of the order of 135 N-m (100 ft-lb). Under certain conditions related to the size of the chamber, moments of inertia of the spacecraft, size and location of the nozzle throat, and position of the motor with respect to the vehicle mass center, the system is unstable, and the amplitude of the nutation increases with time. This growth is further enhanced if the burning period of the motor is long, giving the small torques sufficient time to measurably affect the vehicle dynamics.

The main contribution of Reference 1 was the establishment of the jet gain mechanism just described. Emphasis in the research was on the physical description of the phenomenon and on simple laboratory experimentation aimed at clarification of key issues. Although it was beyond the scope of the original study[1], the gasdynamic model was applied to several actual spacecraft/motor designs in a predictive mode to test its ability to serve as a design tool. Although a very simplified representation for the complex motor geometry and internal flow field was used (chamber shape was simulated by a best-fit cylinder), the results indicated fairly good overall agreement with actual flight data. For example, as Figure 2 demonstrates, the general agreement for final cone angle is acceptable.

Predictions were consistent for several different systems without the need to "curve-fit" the data indicating that scaling is properly accounted for. Only actual spacecraft and motor parameters were used. It must be mentioned that it has been possible to show similar convincing predictive results using other proposed mechanisms. An important test of the validity of such results is their ability to predict behavior of systems with quite different mass properties and motor geomtry.

Reference 1 shows that the coning growth rate and final cone angle are dependent on the parameters shown in Table 2. These were tentative assessments based on an overly simple model of the actual geometry and can only be used as a guide for the more detailed work to be carried out later. It is of some importance to notice that the existence of these sensitivities suggests that careful attention to system design features will make it possible to avoid nutation instability at its source.

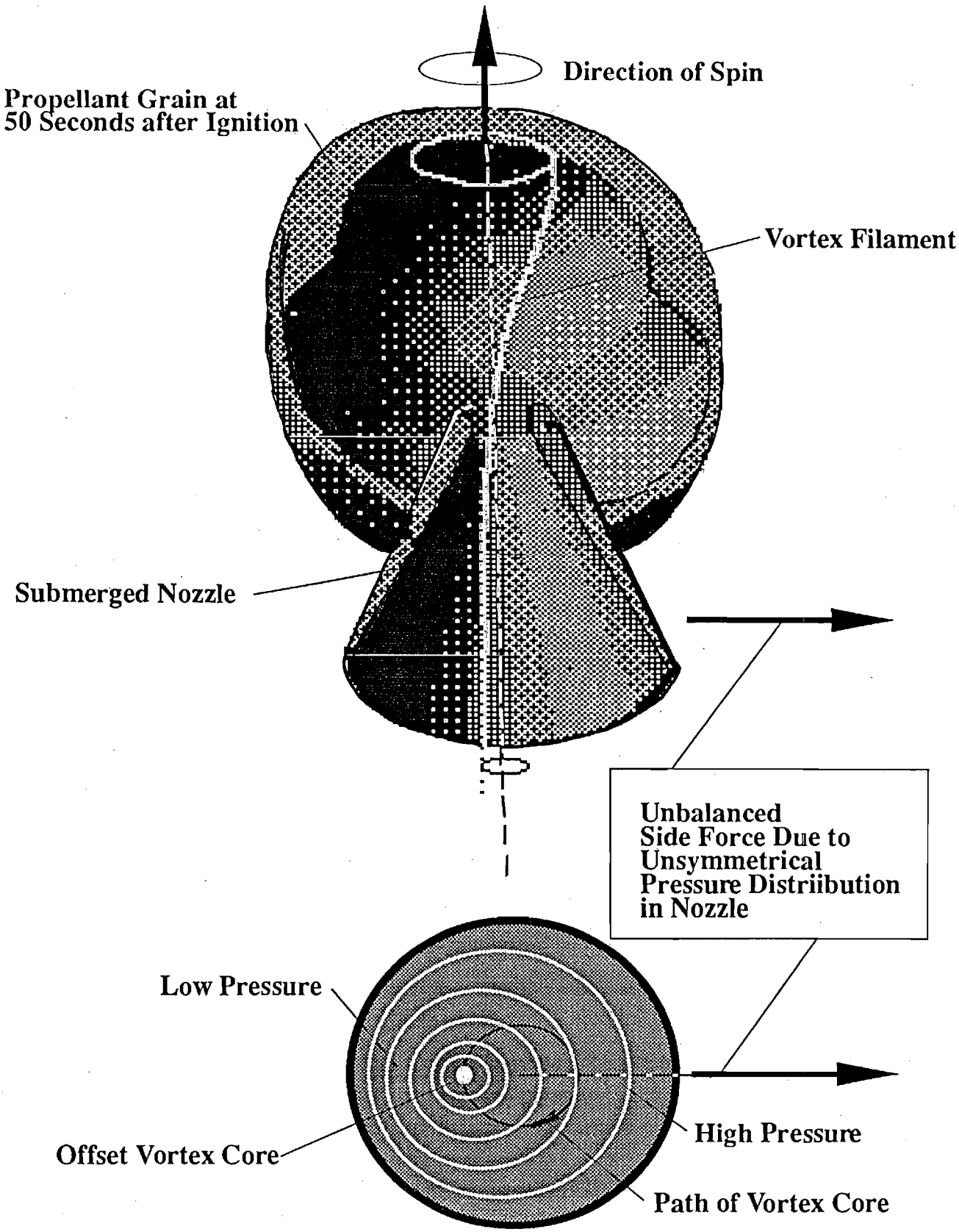

Figure 6. Disturbing Force Due to Unsymmetrical Pressure Pattern in Nozzle

Table 2

SENSITIVITY OF CONING TO SYSTEM PARAMETERS

Parameter	Affect on Coning Instability
Spacecraft Rate of Spin	Growth of final cone angle depends directly on spin rate. Nutation growth is zero at zero spin rate.
Initial Nutation Amplitude	Final cone angle depends directly on the residual nutation amplitude at the beginning of motor run.
Lateral Moment of Inertia	Final coning amplitude depends inversely on lateral Spacecraft moment of inertia, I_1.
Roll Moment of Inertia	Ratio of roll and lateral moments of inertia determines frequency of wobble.
Spacecraft Mass	No evidence of sensitivity to vehicle mass. Thus no indication of acceleration effects.
Motor Burning Time	For given growth rate, final cone angle is larger for longer period of motor operation.
Motor Size	Larger distance between burning surface and nozzle affects coning amplitude and timing of growth.
Mass Flow Rate	Amplitude of disturbing torque is directly proportional to mass flow rate of combustion gases.
Nozzle Throat Size	Torque amplitude is inversely proportional to the square of the nozzle throat radius.
Nozzle Submergence	Location of nozzle entrance directly affects torque amplitude.
Combustion Chamber Shape	More oblate shape reduces growth. Effects of shape of grain contour not known.
Pressure Coupled Responseof Propellant	Growth rate does not seem to be affected by burning rate sensitivity to chamber pressure fluctuations caused by time-dependent combustion response.

Current Status of the Nutation Instability Problem

At the time of writing there are two surviving coning mechanisms (the slag sloshing and the gasdynamic models) out of a very long original list. Support for the flexible nozzle hypothesis has disappeared. A fluid flow model similar to the jet gain mechanism introduced in Reference 1 is now under study by a group at the Aerospace Corporation, but the status of this work is not known. Similar work aimed at clarification of possible two-phase flow (combustion gas/aluminum oxide) effects with emphasis on possible asymmetry of the time-depedent mass flux from the motor is underway at McDonnell Douglas.

Areas Requiring Further Study

Significant progress was made in the preliminary Air Force study. It enables estimates of nutation effects in given vehicles as carried out in the next section for the Ulysses spacecraft. However, much remains to be done before the nutation instability problem can be considered to be properly resolved. Much additional work will be needed for the establishment of actual predictive design tools and experimental verification techniques to be used in full scale static and flight testing.

Of key importance is the construction of a more detailed computational model that more accurately and completely represents the internal flow field in a spinning, nutating combustion chamber. Analytical methods were stretched to the limit in the previous work, and it became clear that numerical techniques would be needed for accurate solutions. For example, in using classical mode superposition methods based on the combustion chamber inertial wave modes, it was found that a large number of modes are required to produce an acceptable solution to the forced gas motions. The mode frequencies are closely spaced as illustrated in Figure 7 and it is difficult to achieve accurate results. Numerical analyses utilizing finite element or finite difference formulations were initiated in the previous study, but considerable work will be required to enable reliable determination of the mean flow field as well as the time-dependent forced motions of the combustion gases.

It was not possible in the Air Force program to address the details of the flow through the expanding nozzle exit cone. Only simple corrections were introduced in Reference 1 to account for the phase modifications and viscous losses generated within the nozzle. These affect the net disturbing moment and its influence on vehicle motion. There is no question that any model intended to be used in a predictive fashion should include a complete treatment of the nozzle flow as well as the combustion chamber flow field itself. No existing nozzle code or analysis adequately covers the present need. The earlier work by Walters[4] established the sensitivity of the lateral nozzle forces to assymetrical flow entering the converging section. Since such works have all assumed

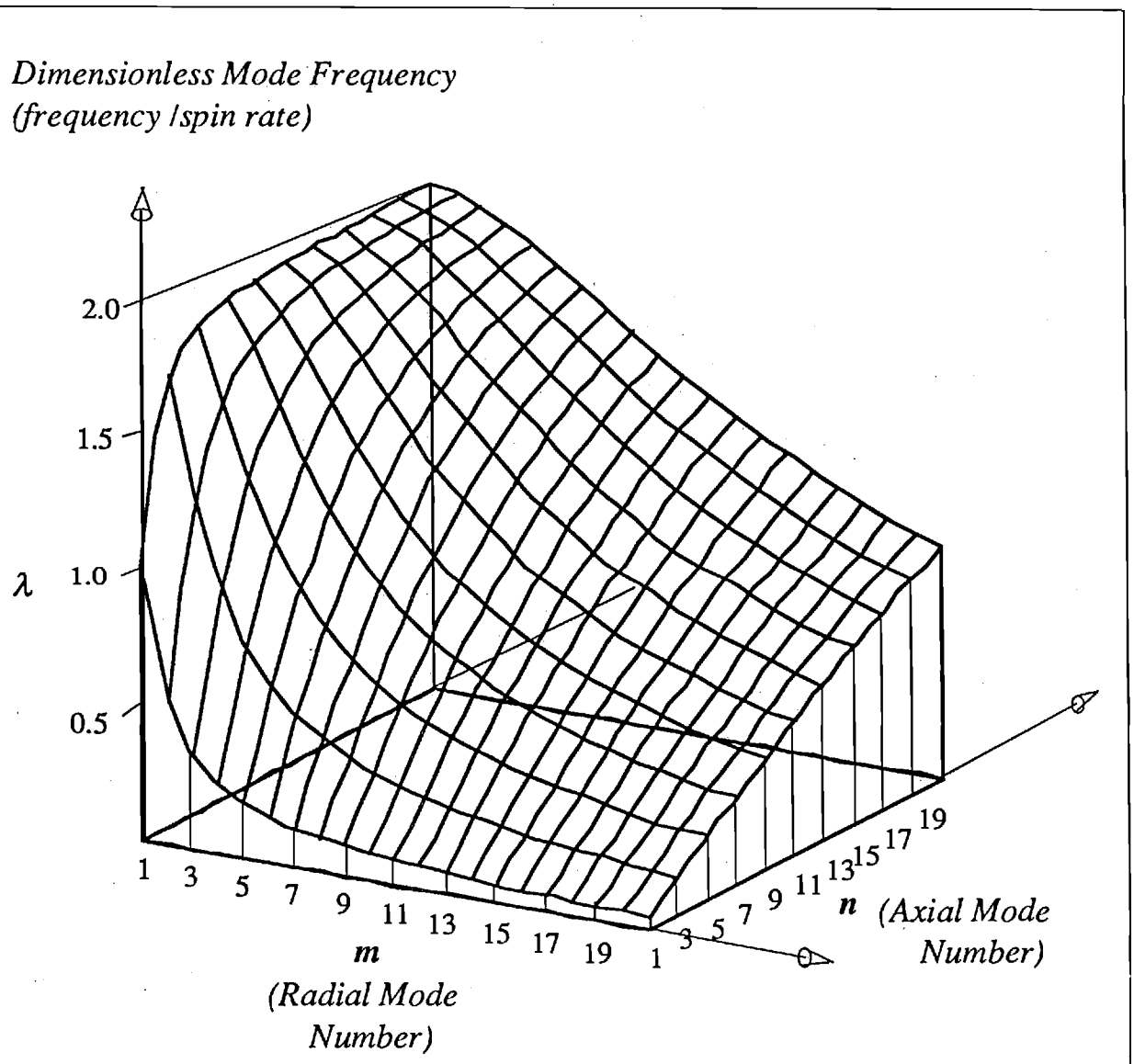

Figure 7. Effect of Mode Integers m and n on Inertial Wave Frequencies

a steady flow, it is essential that a comprehensive three-dimensional, time-dependent nozzle flow field solution be generated.

One of the ground rules adopted in the preliminary program (Ref. 1) was to emphasize physical understanding of spacecraft coning behavior observed in the PAM-D program. For this reason, much reliance was placed on use of perturbation expansions and other simplifying analytical techniques. Use was also made of classical Fourier analysis to represent the forced periodic motion of the combustion gases. These features greatly enhanced the development of a correct physical model for the spacecraft motion. However, the resulting program was not intended for use as a design tool. Some of the elements that require further consideration are:

1. Modeling the complete time-dependent flow field in a geometrically realistic spinning, wobbling motor chamber

2. Inclusion of three-dimensional, time-dependent, compressible nozzle flow including effects of nozzle submergence and details of nozzle entrance geometry

3. More realistic time-dependent combustion model

4. Realistic viscous flow effects especially in vicinity of inert and burning propellant surfaces

5. Effects of compressibility both in nozzle and chamber flowfields

6. Efficient solution algorithms based on state-of-the-art finite difference techniques for the full compressible Navier-Stokes equations including effects of rotating coordinate system effects and evolution of propellant surface geometry with time

There is a pressing need for the identification of practical experimental techniques for the study of spinning rocket fluid dynamics. Continued testing using static test fixutures employing a fixed rotation axis as is currently done is of little direct use in the resolution of the coning problem, although measurement of the body-fixed side forces is helpful. Although the side forces do not lead directly to coning growth, they produce a triggering effect in the presence of a closed loop nutation mechanism such as the jet gain effect.

Useful laboratory scale experimentation is difficult to carry out in spinning systems. Nevertheless, simple measurements can be used to demonstrate basic mechanisms. Both cold flow and small hot motor firings should be employed.

Small Scale Static Motor Testing

With the features of the spinning, nutating rocket problem in mind, it is clear that the first level of experimentation should include laboratory scale rocket motor testing. Application of the preliminary coning model shows that useful verification data can be secured by means of laboratory scale motor tests using a device based on the Froude pendulum concept. A schematic of this device is illustrated in Figure 8. It consists of a small rocket motor mounted to a graphite fiber rod suspended from a universal joint to form a physical pendulum. A small electric motor is also attached to the rod and is used to spin the motor about its axis of symmetry relative to the pendulum structure.

Instrumentation would consist of Kistler pressure transducers arranged to measure pressures in the nozzle throat and at the motor forward end. Sensitive accelerometers or small rate gyroscopes might also be attached to the supporting rod to give direct readouts of system motion. Cabling is routed through the (hollow) rod and through the two orthogonal gimbal components. External optical measurements of motion in laboratory coordinates would also be used to supplement the sensors mounted within the moving system.

A typical run would be started with the motor spinning at a preselected rate and the pendulum swinging with a prescribed initial motion in simulation of nutation. A large initial wobble insures that the internal flow effects responsible for the coning disturbance are immediately activated. The short motor burn (approximately 2 seconds) does not allow development of significant wobbling starting from initially small levels as in actual flight. At this point the motor firing command would be given to start the motor run. Evolution of the angular motion of the Froude pendulum provides data indicating the effects of all external and internal forces and moments acting during motor firing. Gravitational and jet damping effects can be accurately calculated and the residual perturbation gives a direct indication of the effect of internal ballistics interactions. The results would be correlated directly with output from the nutation instability computer code.

Effects of changes in system geometry would be studied in a limited way with this device. For instance, nozzle effects are readily determined by carrying out a set of firings in which changes in nozzle length, expansion ratio, etc. are modified in a systematic fashion. Other key variables in the test matrix would be the pendulum length (to simulate changes in spacecraft lateral moment of inertia) and the axial motor spin rate. High spin rates (of the order of 10,000 rpm) must be utilized to increase the relative amplitude of the gasdynamic nutation disturbing torque according to the scaling rules deduced in Ref. 1.

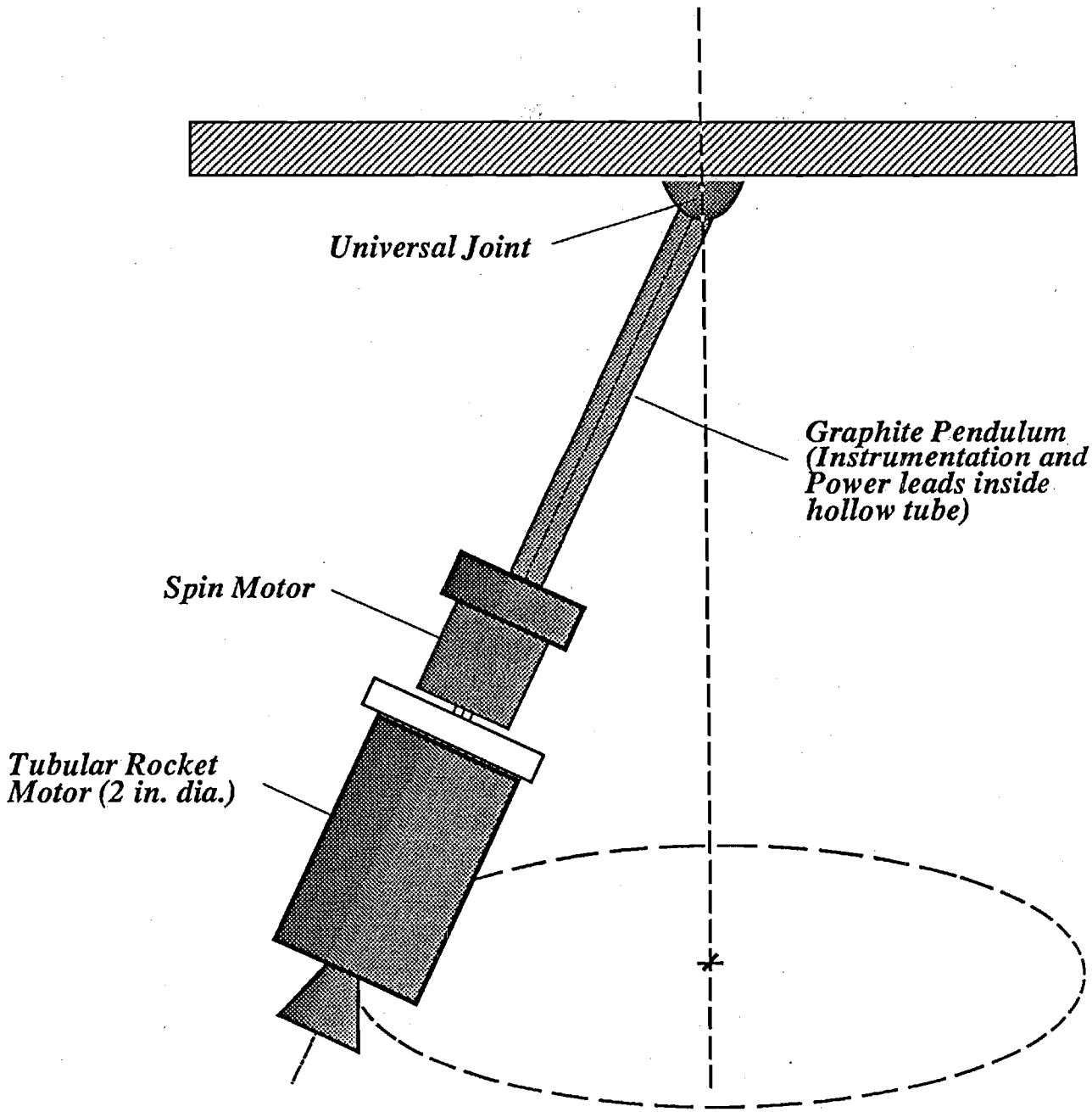

Figure 8. Laboratory Coning Experiment Using Froude Pendulum

Design of Full Scale Verification Static Tests

Resolution of uncertainty in the nutation instability driving mechanism can probably only be accomplished by means of full-scale flight testing. However, it is possible that useful information can be secured in static firings if the motor is mounted in a compliant test stand. Modification of available test facilities might be possible. Figure 9 shows a possible test configuration. There is great need for a carefully engineered instrumentation package that can be adapted to any new spinning motor test program. Both enhanced dynamic data using a high-resolution attitude sensing instrument and motor internal ballistics data using appropriate pressure, temperature, and strain measurements should be developed. A standard set of measurements should be designed that will properly characterize the system nutation stability characteristics.

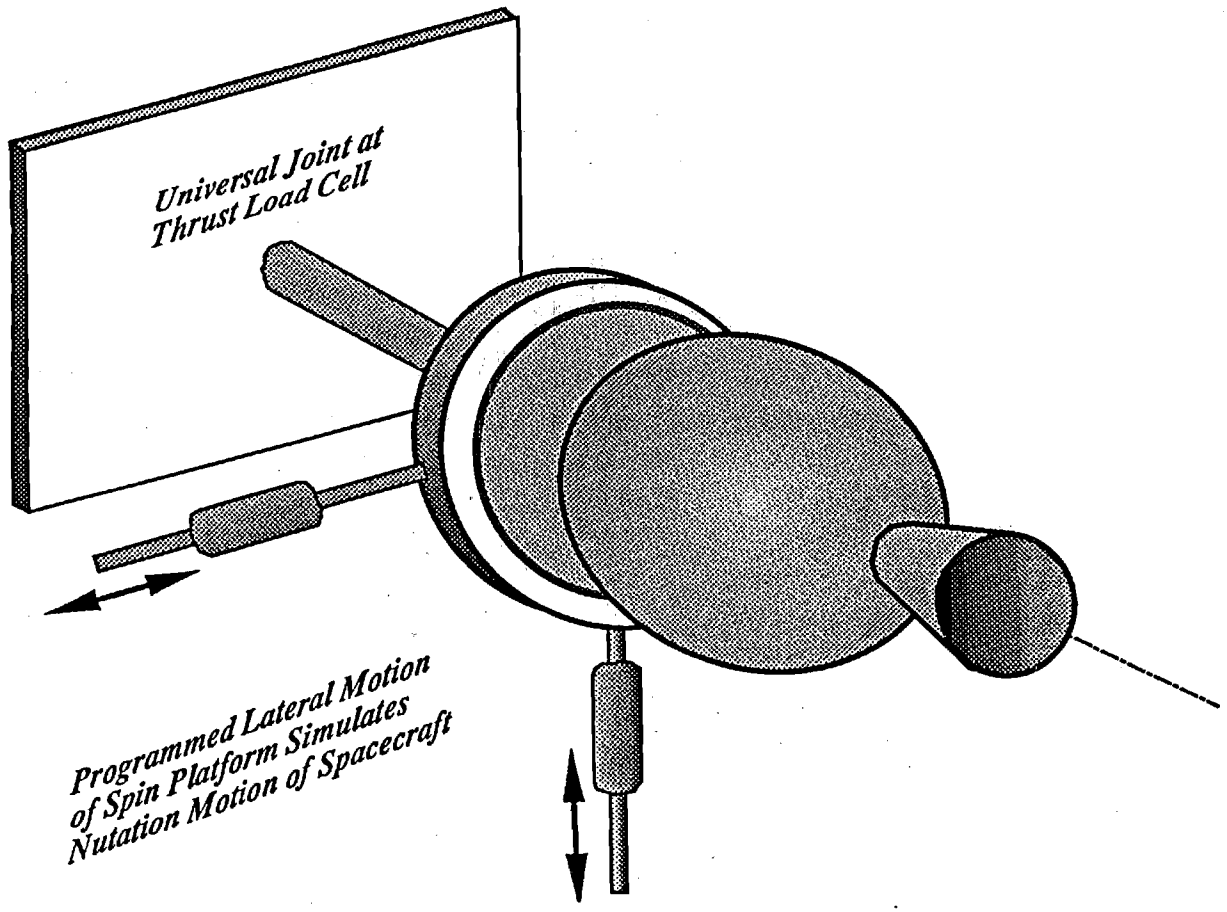

Figure 9. Static Motor Test in Compliant Test Stand

Again, identification of the origin of the nutation disturbance must be made in a completely unambiguous way in order that a reliable attitude control strategy can be established. In high-performance, light weight systems such as the Ulysses design, this is of great importance since the relative loss associated with a large ACS safety factor to account for uncertainties in the nutation disturbance characteristics results in an appreciable payload or performance penalty.

3.0 NUTATION CHARACTERISTICS OF ULYSSES SPACECRAFT

The jet gain nutation instability model described in the last section is now applied to the Ulysses spacecraft design. The computer programs were modified to account for the unequal lateral moments of inertia characterizing this vehicle. Figure 3 shows the moments of inertia plotted vs. time. The data points represent polynomial fits used to represent the variable spacecraft properties in the computations.

The most important features of the Ulysses vehicle in terms of nutation behavior is the relatively small lateral moments of inertia and the correspondingly short motor- to-vehicle mass center distance. The vehicle is also not axially symmetric. The lateral moments of inertia about the center of mass control the responsiveness of the spacecraft to the closed-loop disturbing moments. This effect is illustrated in Figure 2, which indicates that since the Ulysses burnout moment of inertia is about 60% that of a typical PAM-D, a very large final cone angle (approximately 55 degrees) will result if no lateral attitude control is used during the motor burn. The actual cone angle reached depends also on the initial angular rates at motor ignition and on the pattern of body fixed side forces present during the burn. The motor position relative to the mass center is the main parameter controlling the size of the disturbing torque at a given lateral wobbling rate. The theory (see Ref. 1) shows that the torque is proportional to the square of the length Lcg, which for convenience is taken to be the distance between the center of mass and the nozzle exit plane. This length is roughly 80% of the typical PAM-D value resulting in a smaller destabilizing torque. Nevertheless, the low moment of inertia effect is of overwhelming importance; it will become clear that an attitude control system is essential. However, the angular impulse needed to control the nutation is relatively small, and it should be possible to use a light-weight system.

Nutation Instability Algorithm

No attempt will be made here to describe the *Jet Gain* mechanism and the accompanying mathematical analysis in detail. The reader is referred to Reference 1 for a complete description. The computer code used to generate the data presented herein is an improved version of the one developed in the Air Force program. The code generates gain factors representing the system response to vehicle motions. Of most importance in assessment of nutation effects is the parameter to be referred to as *Rgain*, following McDonnell Douglas nomenclature. It is the factor of proportionality between the lateral angular velocity vector describing the wobbling motion and the net reaction torque applied to the vehicle. A positive *Rgain* represents a torque acting in the same sense as the angular velocity vector. This produces a destabilizing effect. A negative *Rgain* yields a stabilizing influence, which adds to the jet damping effect. The gas response is not in phase with the wobbling, and hence there is another component of the disturbing torque normal to the instantaneous direction of the angular velocity perturbation vector. This

component is similarly described by a gain factor Sgain, which does not affect system stability directly. Its presence is indicated by shifts in nutation frequency away from the spinning rigid body value. Its amplitude is always strongly correlated with the Rgain effect as will be demonstrated later.

The following information is required for assessment of nutation instability characteristics of a given vehicle:

1. Motor chamber dimensions and geometry
2. Burnback profiles as functions of time through burn
3. Overall spacecraft mass properties as functions of time throughout burn
4. Estimates of residual nutation rates at end of pre-ignition coast phase
5. Location of vehicle center of mass as function of time
6. General spacecraft layout including placement of motor
7. Nozzle geometry
8. Combustion chamber internal ballistics parameters(mass flow rate, burning rate, mean chamber pressure, speed of sound or mean temperature, specific heats of combustion gases, etc.)

Most of the parameters are fairly smooth functions of time, and are represented by polynomials in the computer program. The program generates a table of gain values, and scaling parameters as functions of burn time. These are then used in a separate simulation program to assess the vehicle nutation behavior. Effects of initial conditions at ignition and body-fixed side forces can be treated parametrically.

The spacecraft model used in the simulations is based on the assumption of a rigid axisymmetric vehicle. The moments of inertia are I_x and I_y about the lateral axes and I_o about the roll axis. These and the vehicle spin rate Ω are assumed to vary slowly with time. The motion is described in the body-fixed coordinate system shown in Figure 10 by Euler's equations:

$$
\begin{aligned}
I_x \frac{d\omega_x}{dt} &= \Omega(I_y - I_o)\,\omega_y + s\,Sgain\,\omega_y + (Rgain + Jgain)\,\omega_x + L_{cg} F_y \\
I_y \frac{d\omega_y}{dt} &= -\Omega(I_x - I_o)\,\omega_x - Sgain\,\omega_x + s(Rgain + Jgain)\,\omega_y - L_{cg} F_x
\end{aligned}
\qquad (2)
$$

Note: M is the reaction moment due to all interactions between the motor flowfield and the vehicle dynamics. Only components parallel to the lateral angular velocity vector ω can affect the growth or decay of nutation. There may also be a component in the z-direction (not shown) that alters the spin rate.

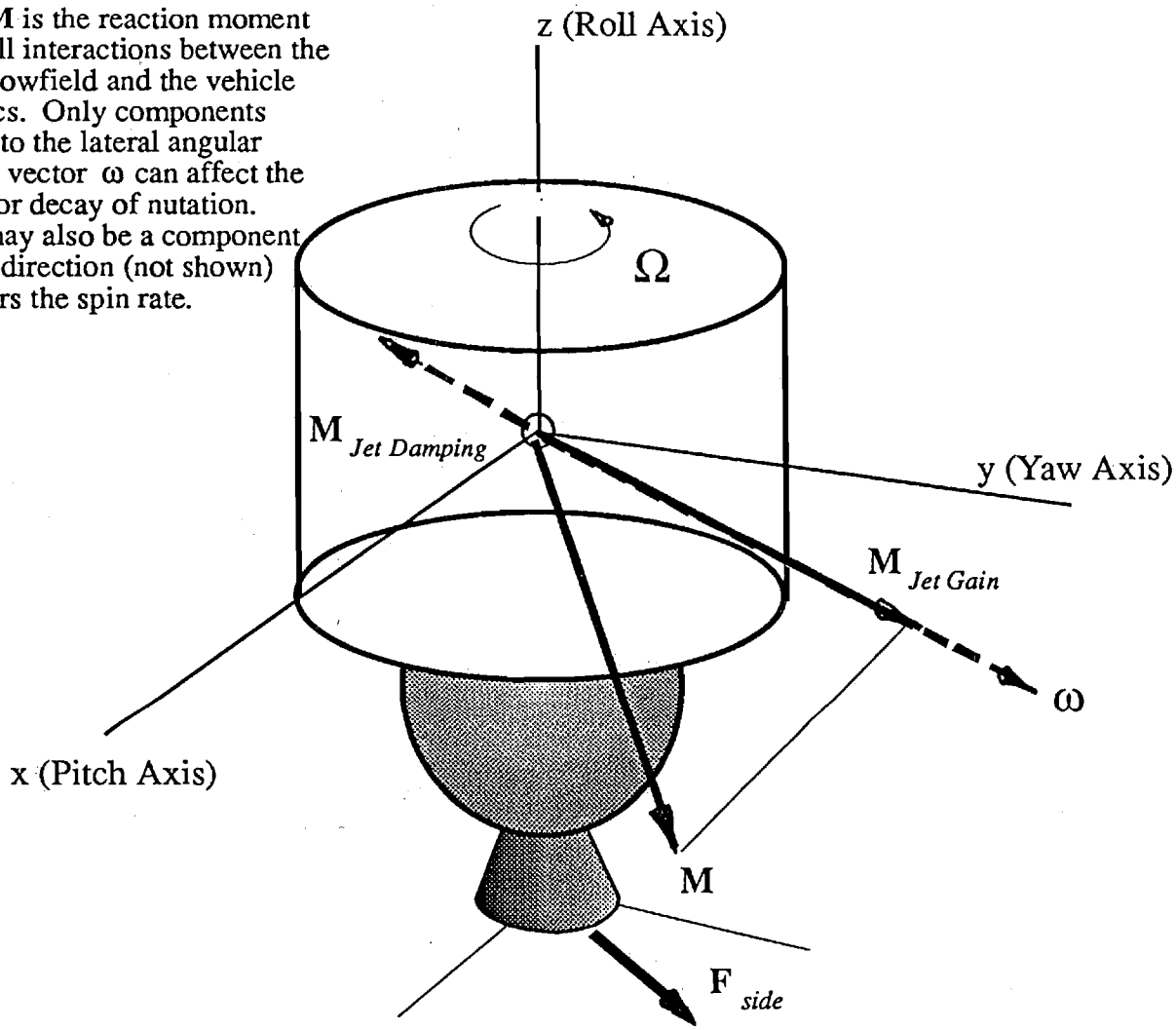

Figure 10. Spacecraft Body-Fixed Coordinate System

The factor s, given by $s = \sqrt{\frac{I_y - I_o}{I_x - I_o}}$, is the effect of the unequal lateral moments of inertia. The reaction moment due to dynamic interaction with motor gas flow is

$$\mathbf{M}_{Jet\,Gain} = Rgain(\mathbf{i}\omega_x + \mathbf{j}\, s\, \omega_y) \tag{3}$$

and the jet damping moment vector is

$$\mathbf{M}_{Jet\,Damping} = Jgain(\mathbf{i}\omega_x + \mathbf{j}\, s\, \omega_y) \tag{4}$$

Jgain is always a negative number. The system is unstable only if *Rgain* is positive and greater than *Jgain*. The x and y axes will be referred to as the pitch and yaw axes respectively. Provision is also made for the presence of a body-fixed side force as shown in equations (2). Thisis assumed to act in the nozzle exit plane as shown in Figure 10, and to change slowly in magnitude and direction with time during the motor burn.

Application of Results to Typical PAMVehicle

Since a simplified representation of the motor chamber geometry is used, the predicted time-history of the gain factors does not match exactly that observed experimentally. However, it is a good representation on the average, and has proven to be a reliable measure of the vehicle coning characteristics. To illustrate these points, the model is first applied to a vehicle from the PAM-D series, the WESTAR-V. This will demonstrate the degree to which it predicts the actual spacecraft behavior.

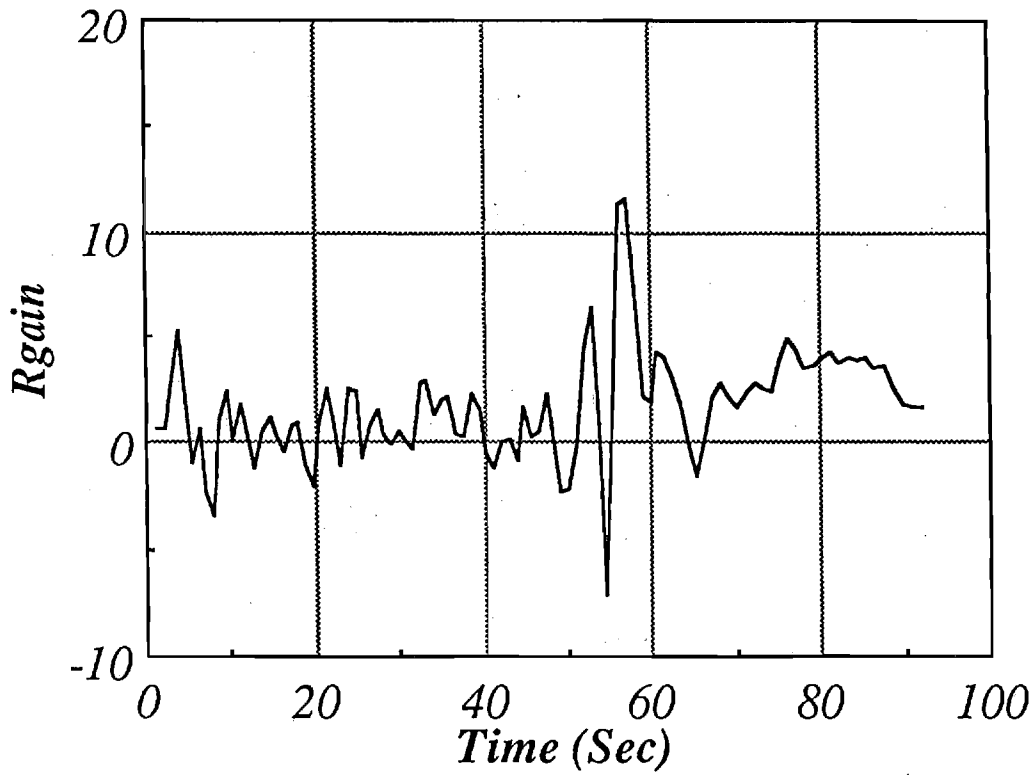

Figure 11. WESTAR-V Rgain vs Time

Figure 11 shows a plot of *Rgain* determined from digitized spacecraft (WESTAR-V) rate gyroscope data. The mathematical model for the spacecraft motion given in equations (2-4) was utilized. The noise in the data comes both from the digitization process used to take the data from printed documents and from telemetry and instrumentation effects.

A feature that is present in all PAM-D coning data is the transient appearing between 50 and 60 seconds after ignition. This consists of a rapid fluctuation in *Rgain* between large positive and negative peaks. Lesser transients can be seen throught the motor burn. The effect of this disturbance is readily seen in most of the PAM-D data as an intial blossoming of the nutation rate before the final sustained growth in the last 15-20 seconds of motor operation. Although the effective *Rgain* value is more than twice

as large as that associated with the final coning growth, its affect on spacecraft motion is ignored in most modeling efforts. This is because it appears while the moments of inertia are still large and it is present for a relatively short time. However, it produces an angular acceleration pulse that acts as a trigger for the final sustained growth. If it were not present, the final nutation amplitude would be significantly smaller. The precise origin of the 50-second transient is not known, but it could be part of the complex interaction between the vehicle dynamics and motor internal flow. None of the proposed nutation disturbance models predicts this feature of the *Rgain* time-history. The jet gain model predicts a steadily growing *Rgain*. However, the predicted behavior represents a reasonable average *Rgain as* will be shown presently.

Figures 12 and 13 show the side force and the angle it makes with the pitch axis. It was assumed that the sideforce acts at the nozzle exit plane. Its magnitude and direction changes slowly with time. These results are consistent with sideforce measurements made in static test firings and appear to be related to small thrust misalignments or CG offset effects. It is important to note that the sideforce is not directly responsible for the nutation growth. The nutation characteristics make it clear that the disturbing entity must be free to move relative to the vehicle. It is for this reason that gas flow effects and slag dynamics are the only remaining viable nutation mechanisms.

Figure 14 shows the instantaneous growth rate deduced from the digitized WES-TAR V rate gyro data. Again, the large mid-burn disturbance is in evidence. The growth rate in the last ten seconds of burn with magnitude growing to approximately 0.2 inverse seconds is responsible for most of the coning growth. This is emphasized in Figure 15, which shows the actual torque acting on the vehicle as a function of time. Since the nutation mechanism involves a closed-loop feedback effect, the reaction moment does not grow to a large value until the last few seconds of motor operation. The final torque of the order of about 100 ft-lbf. is consistent with all PAM-D observations. The figure makes it clear why the mid-burn disturbance is often ignored in attempting to model the nutation mechanism. Although the *Rgain* is large in the 50-60 second time period, the lateral moment of inertia is still large because of the remaining unburned propellant. Thus the effect on nutation growth is relatively unimportant. However, from the standpoint of pinpointing the physics of the nutation mechanism, it is important to look for disturbing effects that are present throughout the motor burn. This is one of the weaknesses of the slag dynamics model, since the disturbing torque gain is critically dependent on the amount of slag accumulated. The amount present at mid-burn is not adequate to account for the 50-second transient. Gas flow effects are affected mainly by the combustion chamber size and shape and the CG position. Thus they are more likely to be effective in producing nutation disturbances earlier in the motor burn. The only feature of the motor grain geometry that correlates with the 50-second transient is the rapid depletion of the sidewall grains. The transition to an end-burning grain takes place in this time period. One might speculate that internal disturbances in the gas flow related to local debonding or

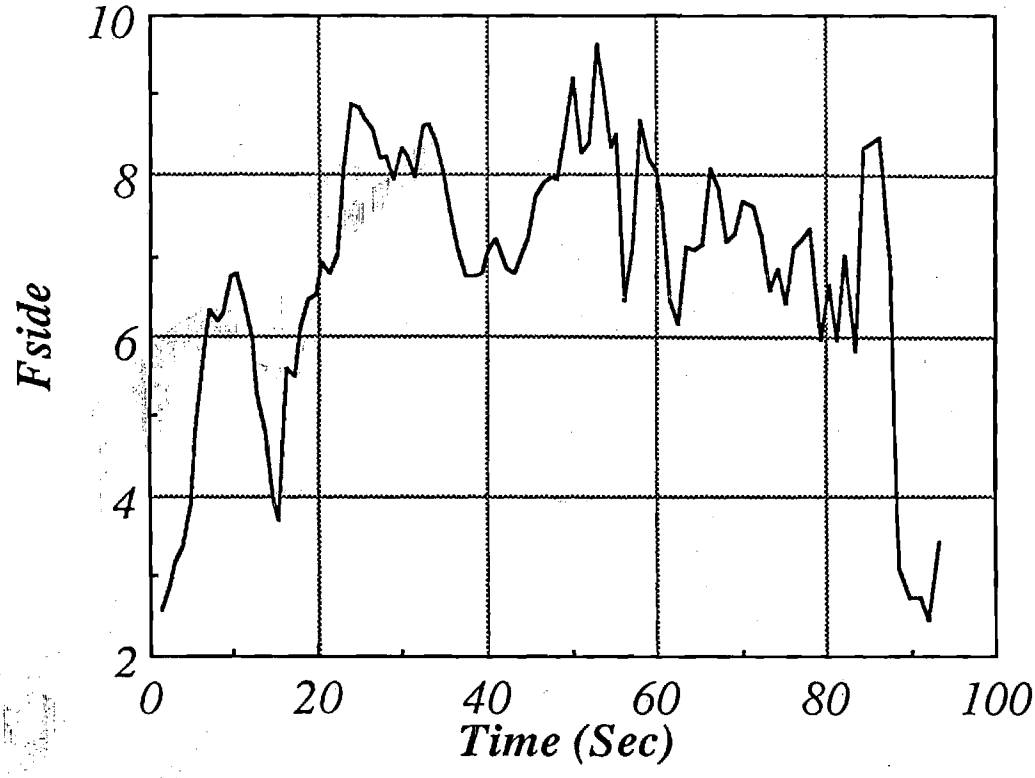

Figure 12. WESTAR-V Sideforce

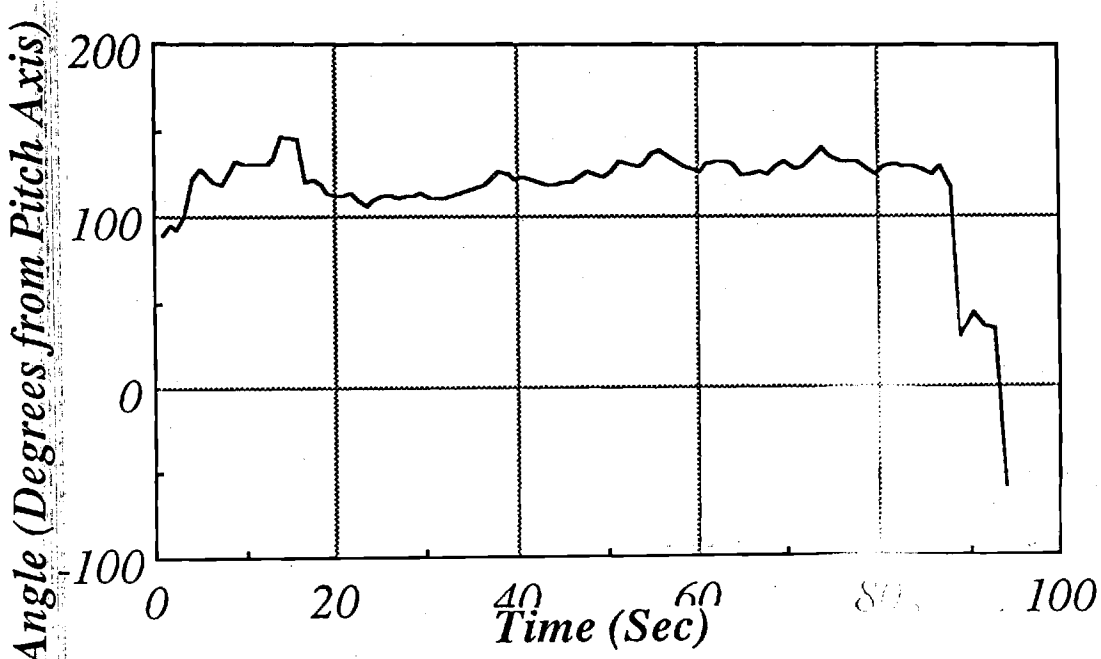

Figure 13. WESTAR V Sideforce Angle

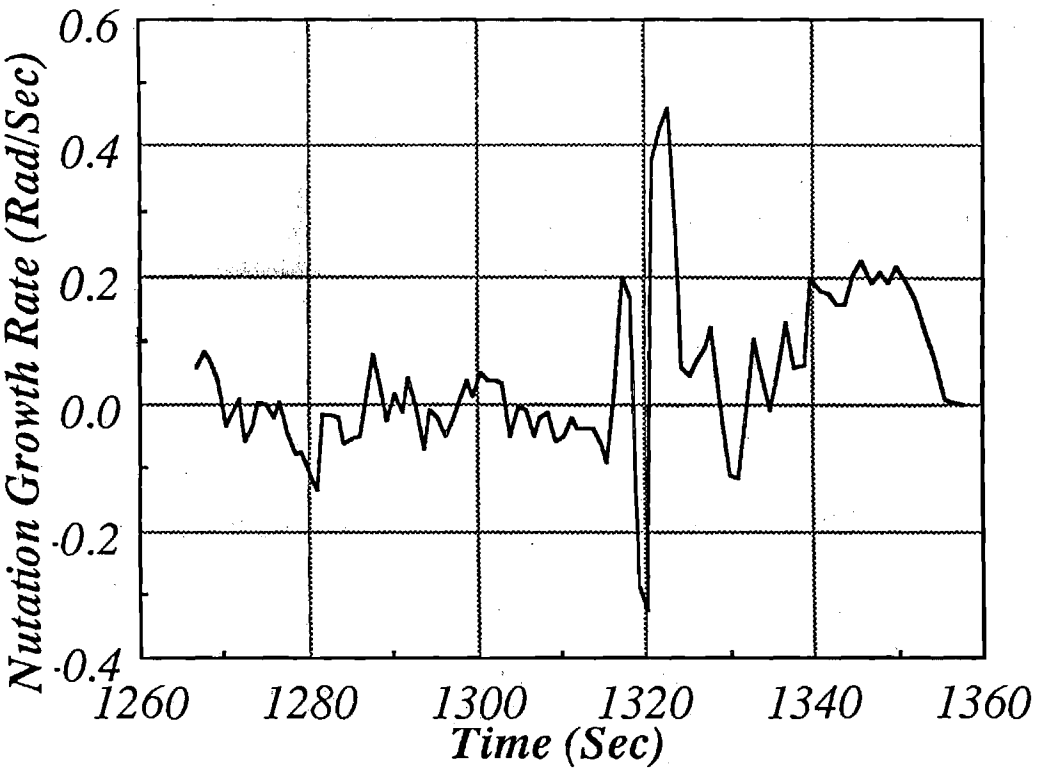

Figure 14. WESTAR V Growth Rate vs Time

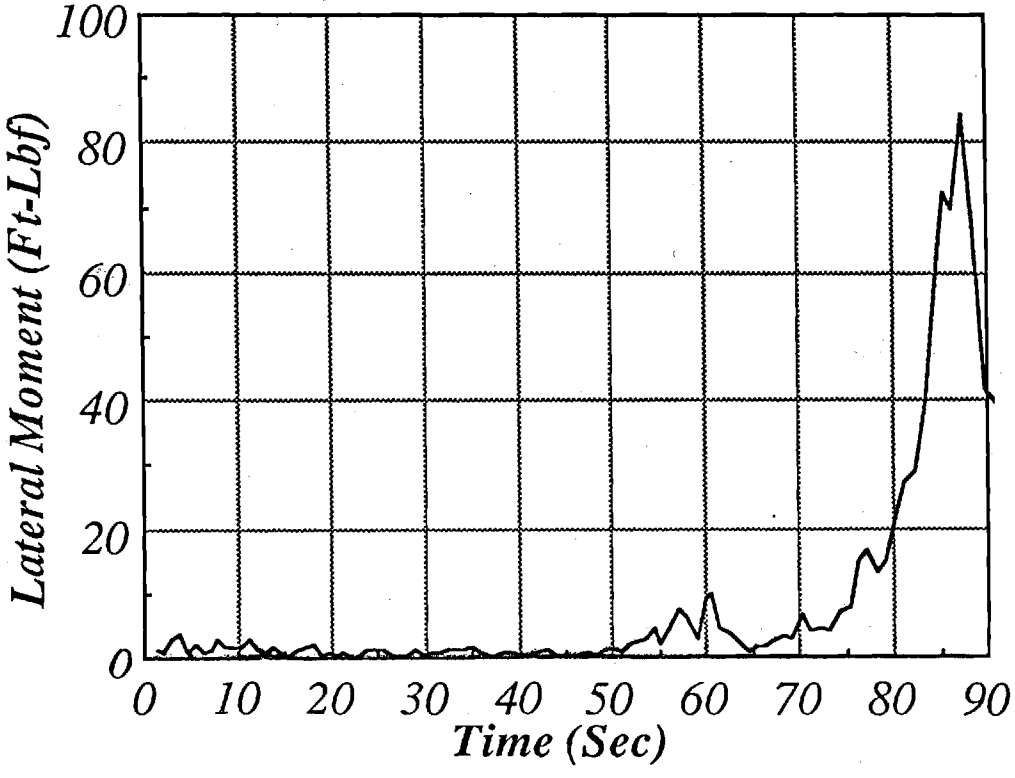

Figure 15. WESTAR V Lateral Disturbing Moment

unsymmetrical regression of the aft edges of the propellant grain could be responsible for perturbing the spinning inertial waves present in the combustion gases. These disturbances would be dramatically amplified in their passage through the nozzle throat because of angular momentum conservation. Resolution of these features of the gas flow must await a detailed numerical analysis. The simplified analytical procedure utilized in Ref. 1 cannot be expected to reproduce fine-detail features of this type.

In order to verify the procedures used to produce the detailed vehicle nutation characteristics summarized in Figures 11-15, equations 2-4 were solved numerically using the side-force and gain information deduced from the rate gyroscope data. One of the features to be tested is the assumption that the rates, moments of inertia, and other vehicle parameters are slowly varying functions of time. The parameters are conveniently represented by polynomials with time as the independent variable when they are sufficiently smooth. The mass center location, Lcg, and the moments of inertia satisfy this requirement. The gain information was accessed by the computer program in table lookup form with linear interpolation between the (closely spaced) data points. Figures 16 and 17 show the pitch and yaw rate information reproduced in this way. The results are virtually identical to the actual rate gyro data. Figures 18 and 19 show enlarged views of the mid-burn transient. Again, the numerically reproduced results are essentially identical to the experimental data except for high-frequency noise, which would not be expected to be recovered. Most PAM-D data contain small high-frequency distortion that is evidently related to structural oscillations of the vehicle. Thus these distortions may represent the (small) effects of vehicle flexibility that are not represented in the rigid body form of Euler's equations (Eq. 2) used in the analysis.

In applying the nutation instability algorithm of Reference 1, one must remember that only an approximate representation for the motor geometry is used. Figure 20 shows how computed Rgain data compare to that deduced from the rate gyro data for WESTAR-V. Three curves are superimposed. The first is the noisy data found directly from the digitized rate gyro data. A smoothed-version of this data is also plotted, which removes some of the noise related to the digitizing process. The third plot is the *Rgain* curve predicted by means of the Jet Gain nutation instability algorithm. Although the latter does not reproduce the fine-scale detail and does not show the mid-burn transient, it generally follows the upward trend of the data and represents a reasonable average of the nutation gain effect. It is for this reason that it produces a fairly good simulation of the vehicle motion as presented in Reference 1.

Application to SGS-II Data

Before using the Jet Gain algorithm for the Ulysses analysis, one additional test of validity is useful. The main difference between the PAM-D and Ulysses vehicles is the difference in mass properties. Thus it is of interest to see if the algorithm properly accounts

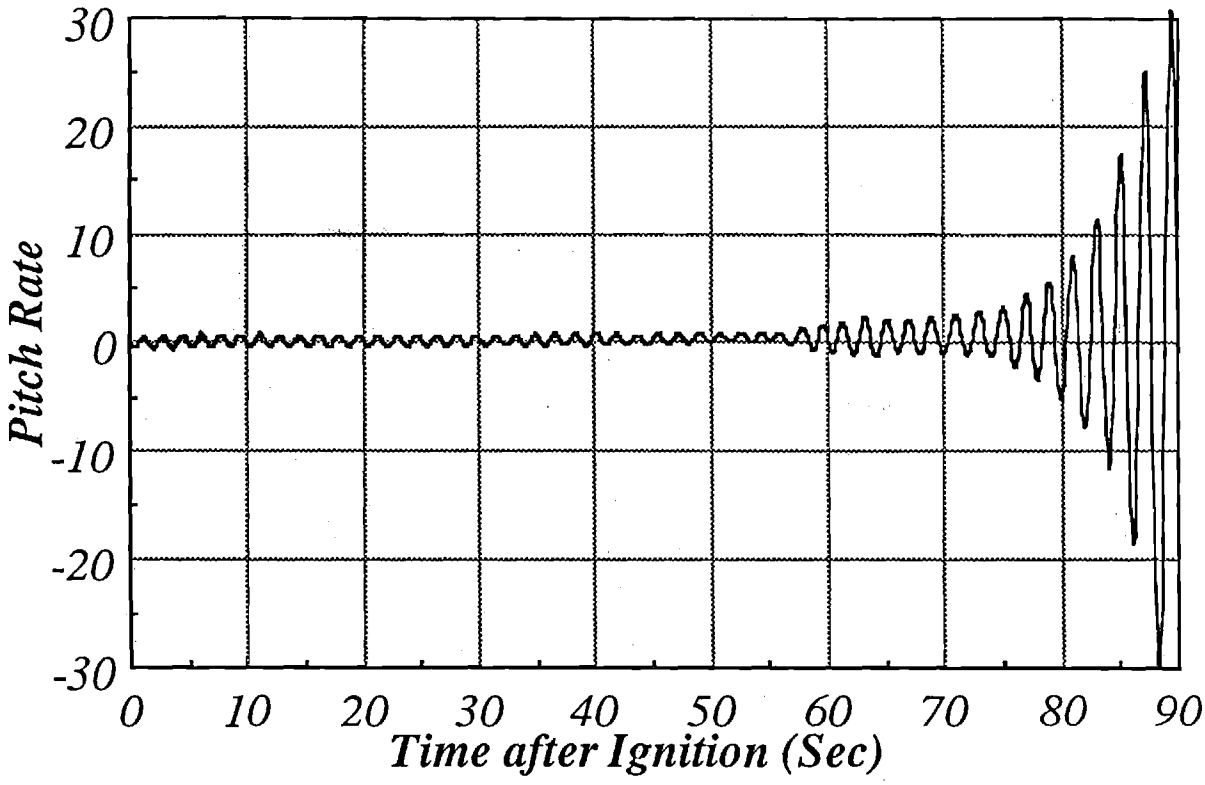

Figure 16. Predicted Pitch Rate vs Time WESTAR V

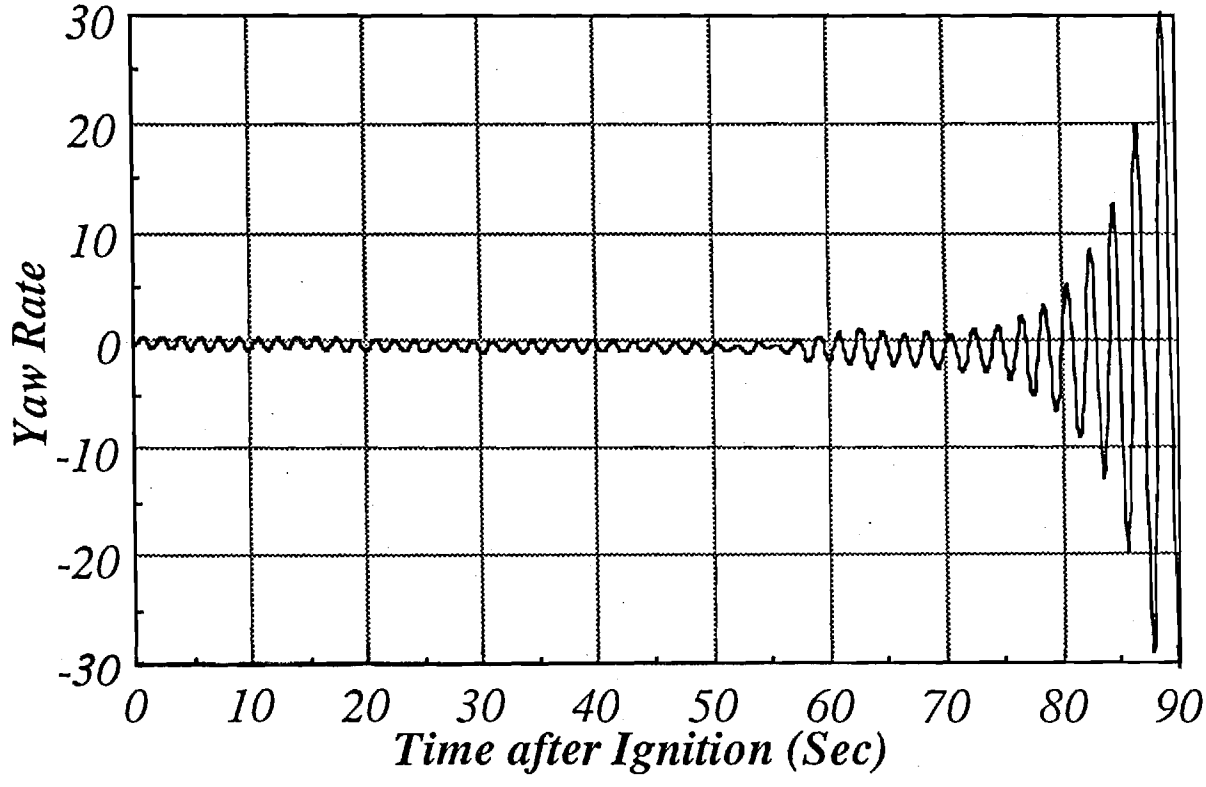

Figure 17. WESTAR V Predicted Yaw Rate

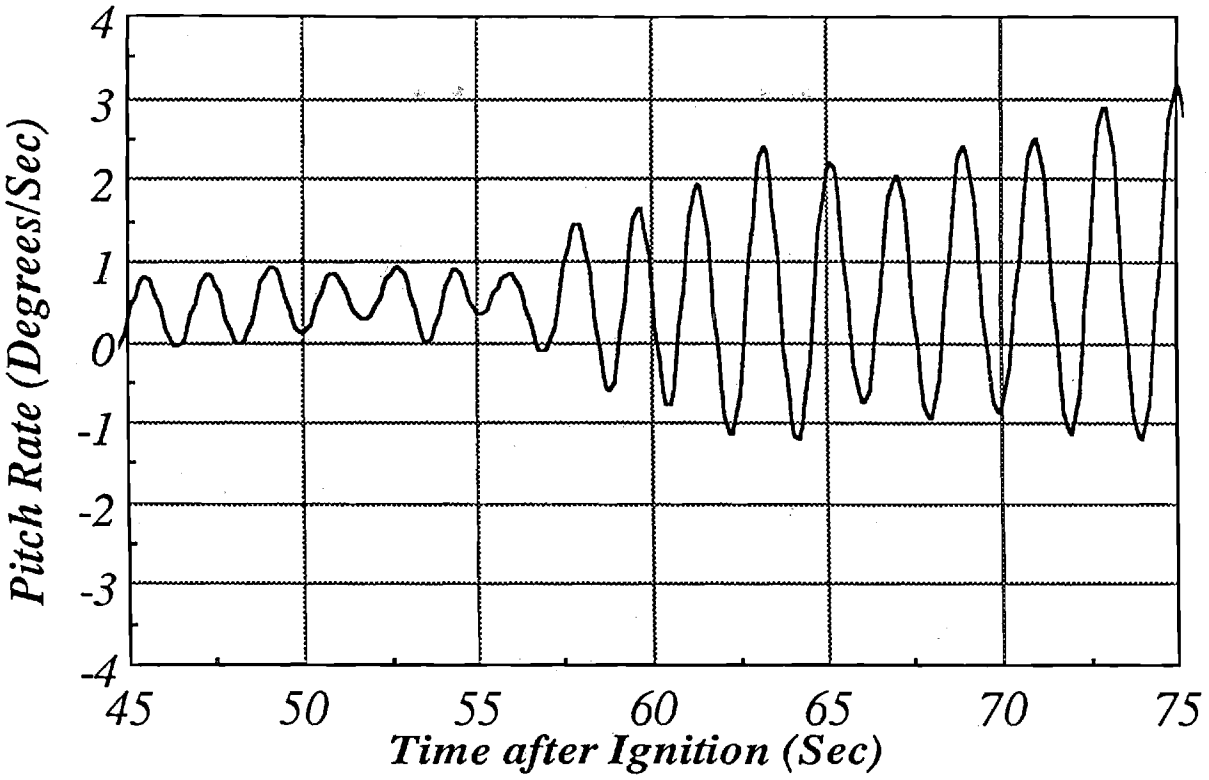

Figure 18. Predicted Pitch Rate vs Time WESTAR V

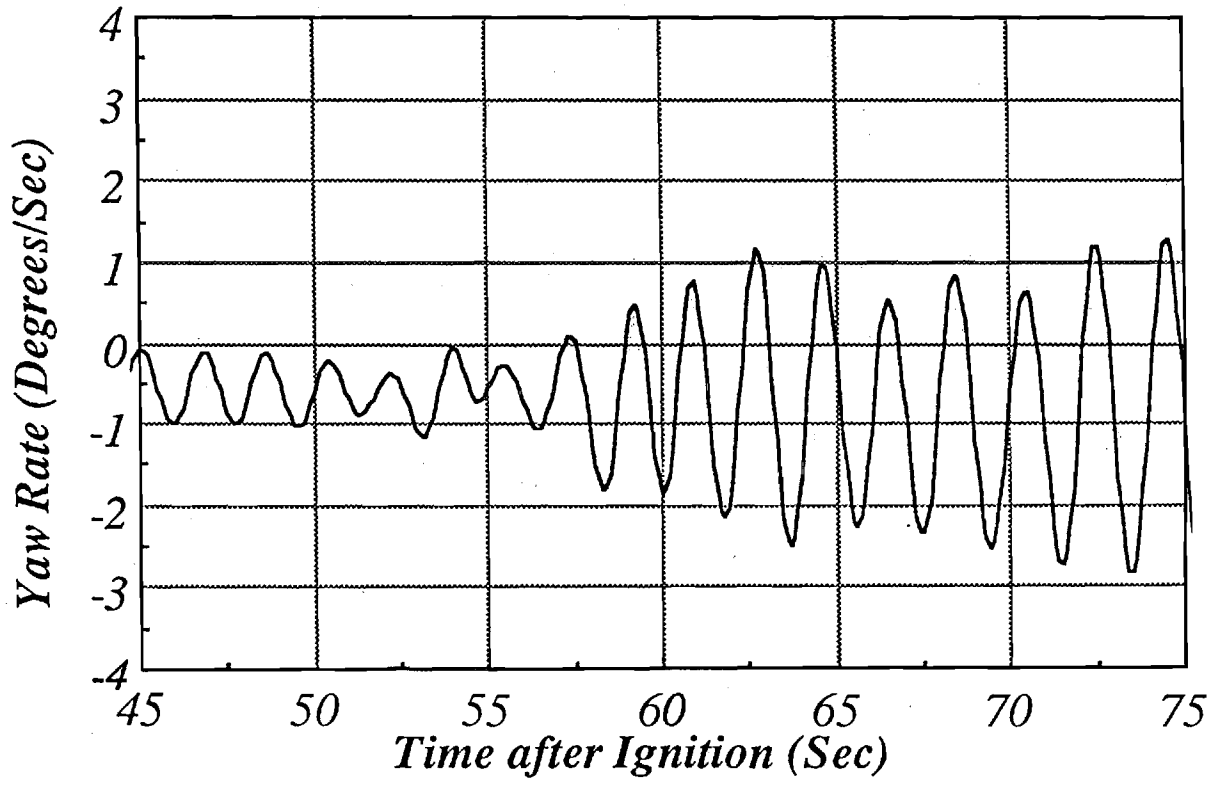

Figure 19. Predicted Yaw Rate vs Time WESTAR V

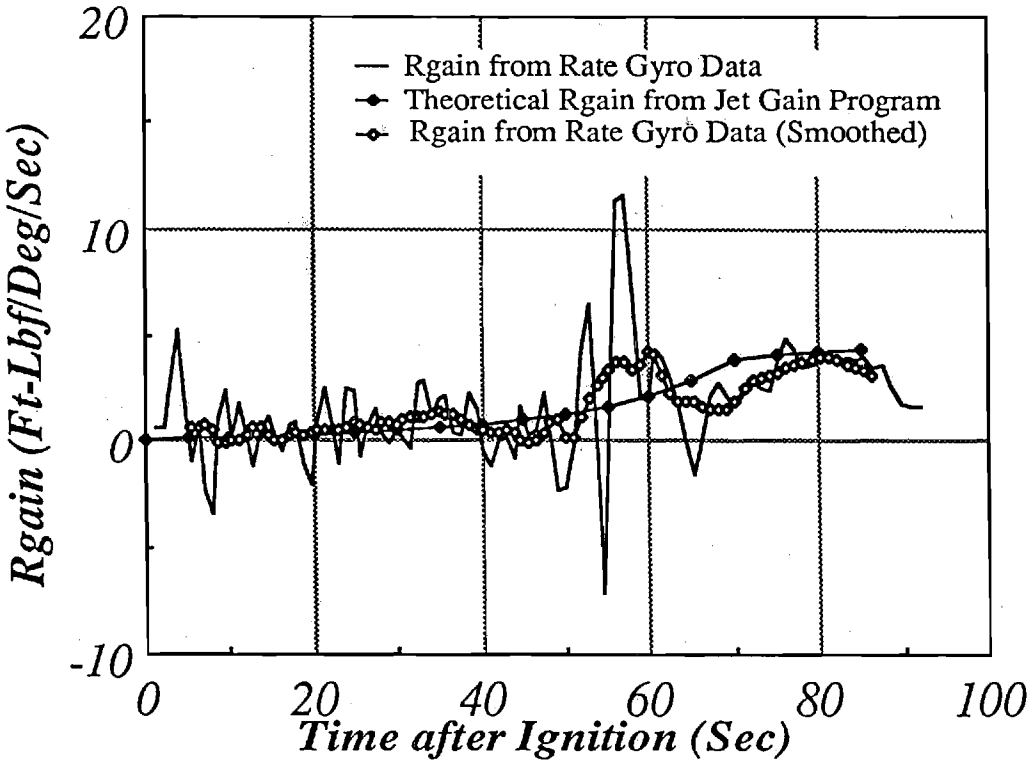

Figure 20. Comparison of Theoretical and Experimental *Rgain* (WESTAR V)

for such differences. The SGS-II stage 1 data can be used for this purpose. These data are usually ignored as a source of information in the coning phenomenon because the nutation amplitude remained very small as a result of the large moment of inertia during the SGS-II stage 1 STAR 48 burn. The amplitude stayed within the 2 degree per second ACS dead band, and the system was not activated. The attitude control system operated during the second stage burn and successfully controlled coning. Nevertheless, all characteristics of the PAM-D coning phenomenon are present in the stage 1 data, and obviously arise from the same source. *Rgain* was determined for the SGS-II, stage 1 (flight 2) by anayzing the digitized rate gyroscope data. This was tested in the same manner used to verify the WESTAR-V data, and the predicted angular rate history is shown in Figure 21. Again, the results closely duplicate the actual rate gyro data. Note that the *Rgain* values are significantly larger than those for WESTAR-V, but follow a very similar pattern. The mid-burn transient is very much like that in the PAM-D observations and must arise from the same source. Figure 22 is a plot of smoothed experimental *Rgain* data with the predicted *Rgain* from the Jet Gain nutation instability algorithm. The theoretical plot does not reproduce the mid-burn transient, but otherwise follows the average trend fairly well. The larger *Rgain* values are mainly the result of the longer moment arm, Lcg, which enters approximately as its square in the calculations. It is significant that the jet damping depends in a similar way on Lcg. Both jet damping and jet gain arise from similar physical mechanisms. However, jet damping is based on the strong assumption of a steady gas flow. Jet gain accounts for the time dependent response of the gas flow to the oscillatory vehicle nutation motion and also incorporates the effects of axial vortex flow through the chamber and nozzle.

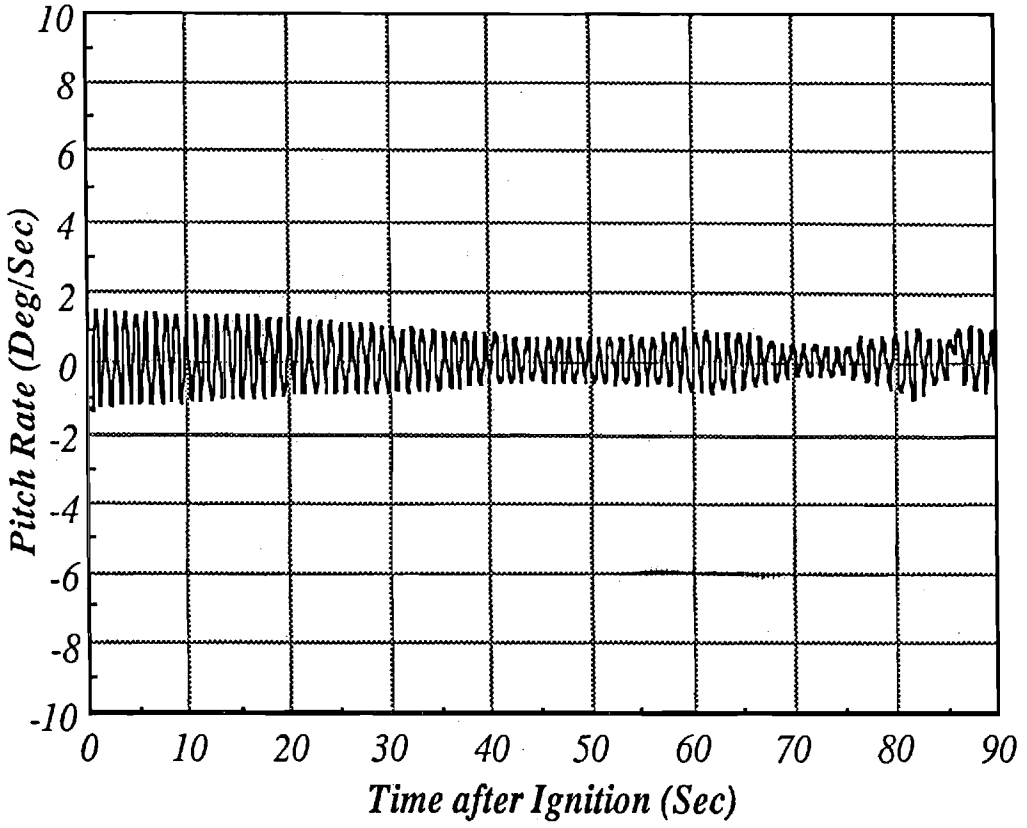

Figure 21. Simulated Pitch Rate vs Time SGS-II (stage 1), Flight 2

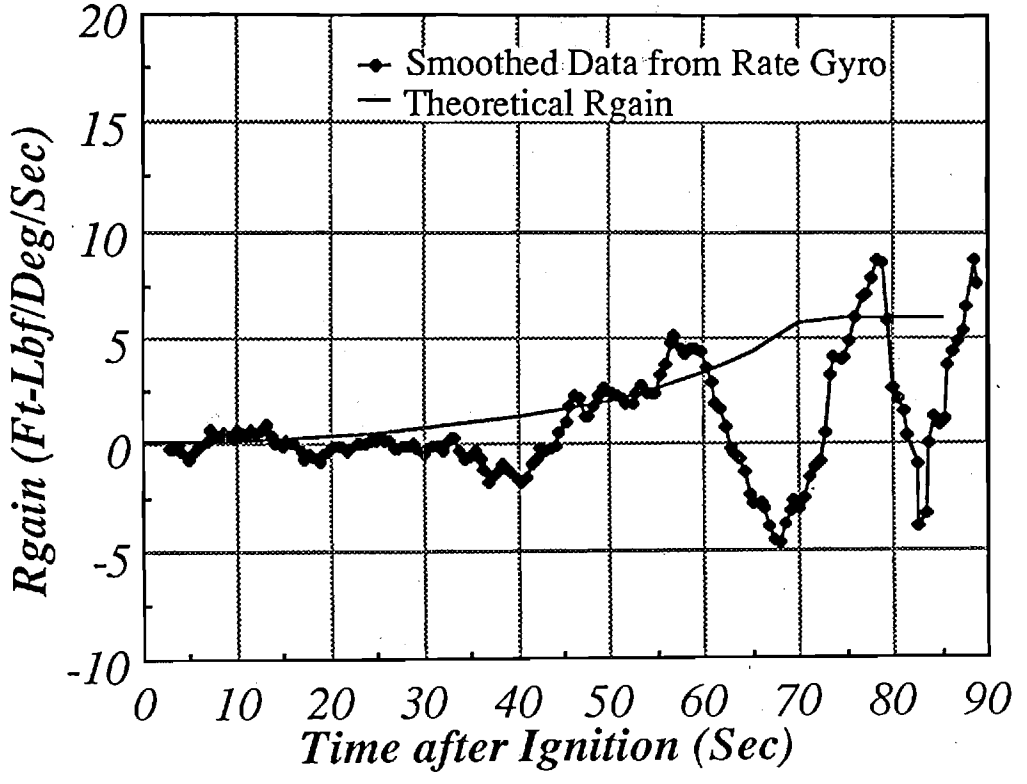

Figure 22. Comparison of Theoretical and Experimental *Rgain*, SGS-II

Application to ULYSSES Spacecraft

The Jet Gain nutation algorithm is now applied in a predictive fashion to the Ulysses configuration. Results are compared to the PAM and SGS calculations to indicate the relative importance of various parameters. Figure 23 is a plot of the time variation of Lcg for the two reference vehicles and the Ulysses. Figure 23 shows one of the main differences between the heavier (SGS and PAM-D) and lighter Ulysses designs. Since the moment arm is considerably shorter for the light-weight spacecraft, the effect of the disturbing torque should be correspondingly smaller since it originates in the vicinity of the motor nozzle. However, this is offset by the higher spin rate of the Ulysses as shown in Figure 24, which is a plot of the predicted *Rgain* vs time for the three vehicles. The gain information is also shown in Tables 3 and 4. The parameters labled kr, ki, and kj (designated K1, K2, and Kj in Ref. 1) are the dimensionless forms of *Rgain, Sgain*, and the Jet Damping factor (*Jgain*) computed in the nutation instability algorithm. The scale factor

$$m_o = \rho_o R_o^4 v_b \Omega \tag{5}$$

is also tabulated. This factor is proportional to the motor mass flow rate since ρ_o is the gas density, v_b is the gas velocity at the burning surface, and R_o^2 is proportional to the burning surface area since R_o is a reference length equal to the effective chamber radius. Ω is the angular velocity of the spacecraft. kr multiplied by this factor and divided by the spin rate yields *Rgain* in radians per second. The tabulated values of the gain factors are in ft-lbf per degree/second units. The Ulysses *Rgain* values are smaller than the PAM-D values mainly as a result of the shorter moment arm. However, the jet damping also depends roughly on the square of Lcg, and is therefore smaller for the Ulysses as plotted in Figure 25.

Although the net driving effect (combination of jet gain and jet damping) is lower for the Ulysses vehicle, the nutation growth rate is larger because the latter is controlled by the vehicle moments of inertia. The instantaneous exponential growth rate is related to *Rgain* by

$$\alpha = \frac{m_o}{2\Omega}\left(\frac{I_y + sI_x}{I_x I_y}\right)(k_r + k_j) \sim \frac{(Rgain + Jgain)}{I_1} \tag{6}$$

and the effect of the lower lateral moments of inertia is indicated. Figure 26 shows the variation of the symmetry factor s with time for Ulysses. Since s does not depart greatly from unity, the second expression in (6) for *Rgain* is a useful approximation. Figure 27 compares the predicted growth rates for the three vehicles. The Ulysses growth rates are roughly twice that of the WESTAR-V. Thus rapid divergence of the vehicle attitude in the last part of the motor run should be anticipated.

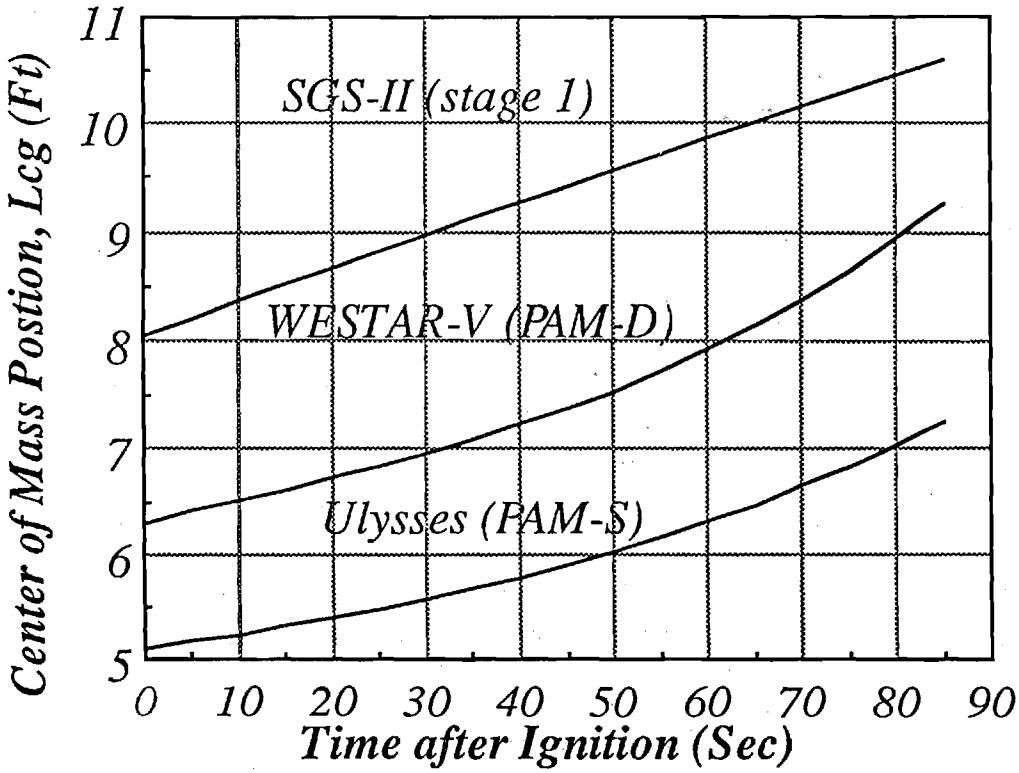

Figure 23. Center of Mass Position vs Time

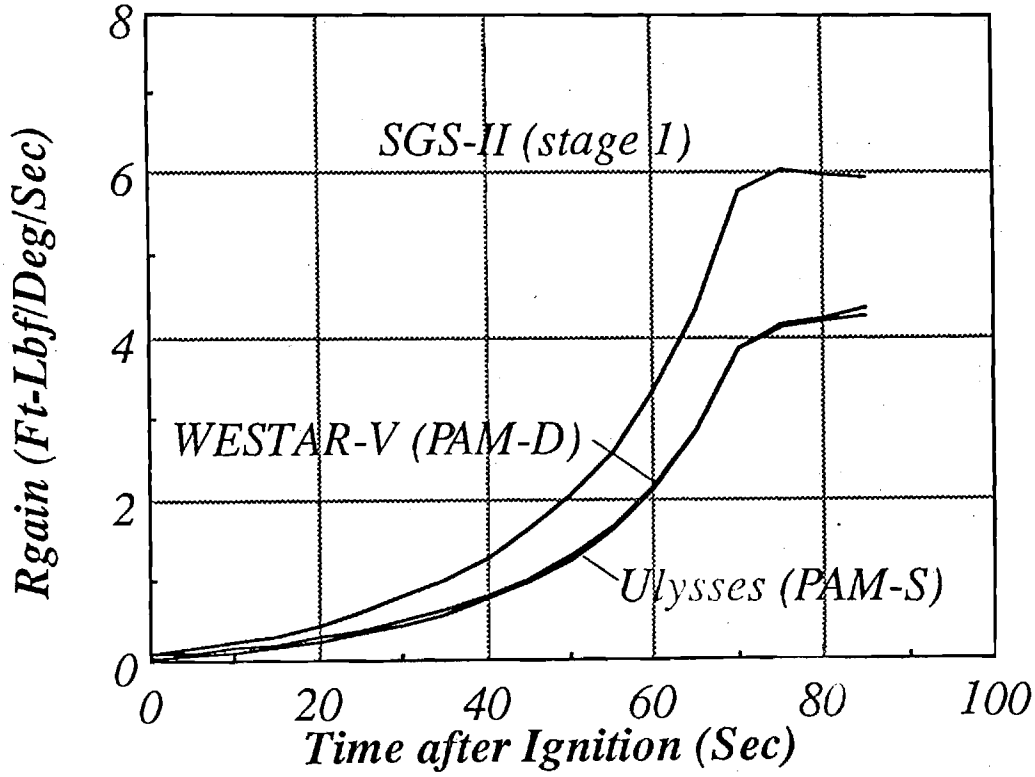

Figure 24. Predicted *Rgain* vs Time

Table 3
STANDARD GAIN DATA

SGS-II (First stage of tandem STAR 48 Air Force system)

t	Kr	Ki	Kj	Omega	Lcg	Mo	Rgain	Jgain	Alpha
0	614.03	132.89	-5318.18	7.01	8.06	0.070	0.107	-0.923	-0.007
5	405.65	71.53	-2573.65	7.02	8.21	0.151	0.152	-0.966	-0.007
10	328.00	52.25	-1505.33	7.02	8.36	0.270	0.220	-1.010	-0.007
15	295.25	44.44	-995.13	7.03	8.51	0.427	0.313	-1.056	-0.007
20	287.10	41.76	-714.92	7.04	8.66	0.622	0.443	-1.103	-0.007
25	280.32	38.32	-544.16	7.04	8.81	0.854	0.593	-1.151	-0.006
30	278.87	35.91	-431.12	7.05	8.96	1.125	0.777	-1.201	-0.005
35	280.19	34.06	-350.90	7.06	9.11	1.443	1.000	-1.252	-0.003
40	283.11	32.55	-290.45	7.06	9.26	1.818	1.272	-1.305	-0.000
45	287.17	31.26	-242.54	7.07	9.41	2.269	1.609	-1.359	0.003
50	292.22	30.16	-203.01	7.08	9.56	2.824	2.035	-1.414	0.009
55	298.35	29.23	-169.44	7.08	9.71	3.523	2.590	-1.471	0.016
60	305.80	28.48	-140.45	7.09	9.86	4.424	3.329	-1.529	0.028
65	314.99	28.00	-115.26	7.10	10.01	5.607	4.343	-1.589	0.046
70	326.65	27.90	-93.44	7.10	10.16	7.190	5.770	-1.650	0.074
75	325.83	26.79	-92.30	7.11	10.31	7.563	6.048	-1.713	0.084
80	322.38	25.62	-95.78	7.12	10.46	7.570	5.984	-1.778	0.089
85	319.72	24.68	-99.33	7.12	10.61	7.577	5.935	-1.844	0.095

WESTAR-V (PAM-D/STAR 48)

0	482.03	153.28	-3775.13	5.38	6.30	0.053	0.084	-0.655	-0.015
5	300.72	70.63	-1824.46	5.37	6.41	0.116	0.113	-0.685	-0.016
10	230.52	47.46	-1065.38	5.37	6.52	0.207	0.155	-0.715	-0.016
15	198.91	38.40	-703.20	5.37	6.62	0.327	0.211	-0.746	-0.016
20	187.30	35.10	-504.63	5.37	6.73	0.475	0.289	-0.779	-0.015
25	179.33	31.80	-383.96	5.38	6.84	0.652	0.379	-0.812	-0.014
30	176.17	29.63	-304.42	5.39	6.96	0.860	0.491	-0.848	-0.012
35	175.75	28.08	-248.29	5.39	7.09	1.103	0.627	-0.886	-0.009
40	177.16	26.90	-206.29	5.40	7.23	1.391	0.796	-0.927	-0.005
45	179.98	26.00	-173.23	5.42	7.38	1.738	1.008	-0.970	0.002
50	184.15	25.33	-146.12	5.43	7.54	2.167	1.283	-1.018	0.011
55	189.74	24.87	-123.18	5.45	7.72	2.709	1.647	-1.069	0.026
60	196.99	24.65	-103.38	5.47	7.92	3.409	2.145	-1.126	0.050
65	206.33	24.74	-86.11	5.49	8.14	4.333	2.845	-1.187	0.088
70	218.44	25.30	-71.04	5.51	8.38	5.574	3.858	-1.255	0.152
75	224.01	24.94	-71.61	5.53	8.65	5.883	4.158	-1.329	0.184
80	228.81	24.57	-76.01	5.56	8.94	5.911	4.247	-1.411	0.209
85	235.08	24.50	-80.87	5.58	9.26	5.940	4.364	-1.501	0.244

Table 4 - Jet Gain Computations
ULYSSES PAM-S Spacecraft

t	Kr	Ki	Kj	Omega	Lcg	Mo	Rgain	Jgain	Alpha
0	260.67	41.50	-2932.86	7.54	5.10	0.075	0.045	-0.509	-0.028
5	193.11	33.16	-1408.55	7.54	5.17	0.162	0.072	-0.529	-0.029
10	166.98	27.32	-818.54	7.54	5.23	0.290	0.112	-0.549	-0.029
15	156.60	24.46	-538.29	7.54	5.31	0.459	0.166	-0.571	-0.027
20	156.67	23.66	-385.24	7.55	5.39	0.668	0.242	-0.594	-0.025
25	155.99	22.07	-292.56	7.56	5.47	0.916	0.330	-0.619	-0.021
30	157.84	20.99	-231.63	7.57	5.57	1.209	0.440	-0.645	-0.016
35	161.19	20.20	-188.73	7.58	5.67	1.551	0.575	-0.673	-0.008
40	165.64	19.61	-156.67	7.60	5.77	1.956	0.744	-0.704	0.003
45	171.06	19.17	-131.46	7.62	5.89	2.445	0.958	-0.736	0.020
50	177.51	18.86	-110.78	7.64	6.02	3.049	1.236	-0.772	0.043
55	185.13	18.67	-93.27	7.66	6.16	3.811	1.607	-0.810	0.078
60	194.21	18.64	-78.15	7.69	6.31	4.796	2.114	-0.851	0.131
65	205.16	18.82	-64.95	7.72	6.47	6.095	2.828	-0.896	0.212
70	218.68	19.33	-53.44	7.75	6.65	7.839	3.863	-0.944	0.338
75	223.31	18.83	-53.68	7.78	6.84	8.273	4.145	-0.996	0.385
80	226.11	18.25	-56.60	7.81	7.04	8.311	4.197	-1.051	0.406
85	229.23	17.88	-59.38	7.85	7.26	8.350	4.255	-1.102	0.428

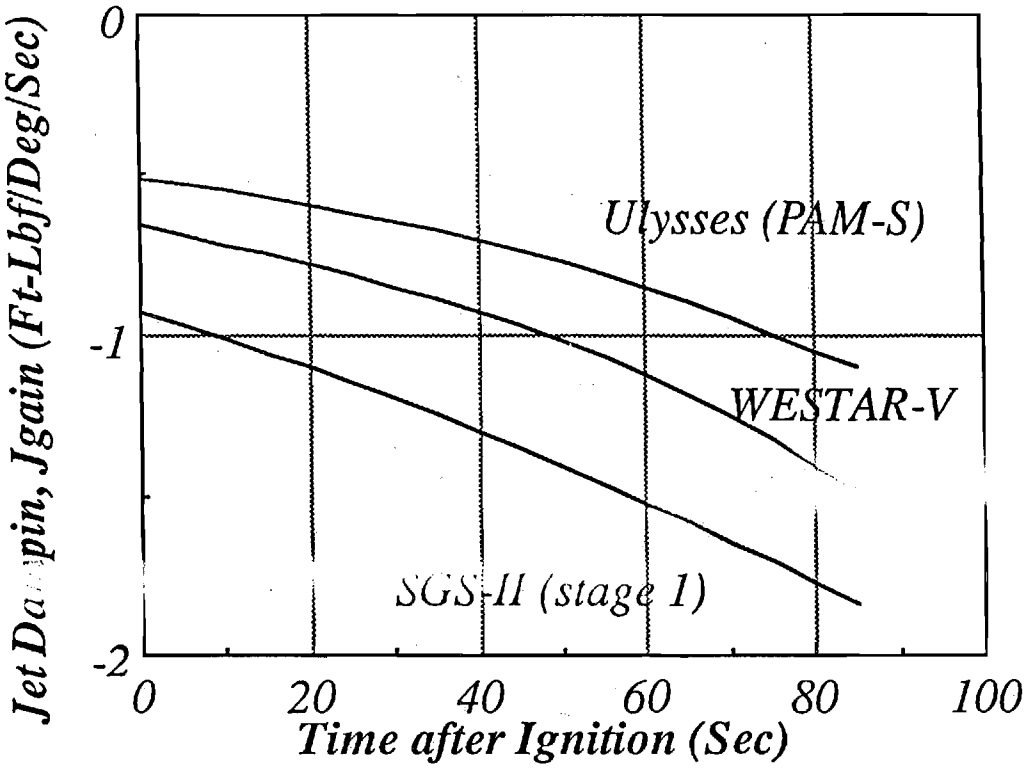

Figure 24. Predicted *Rgain* for Several Vehicles

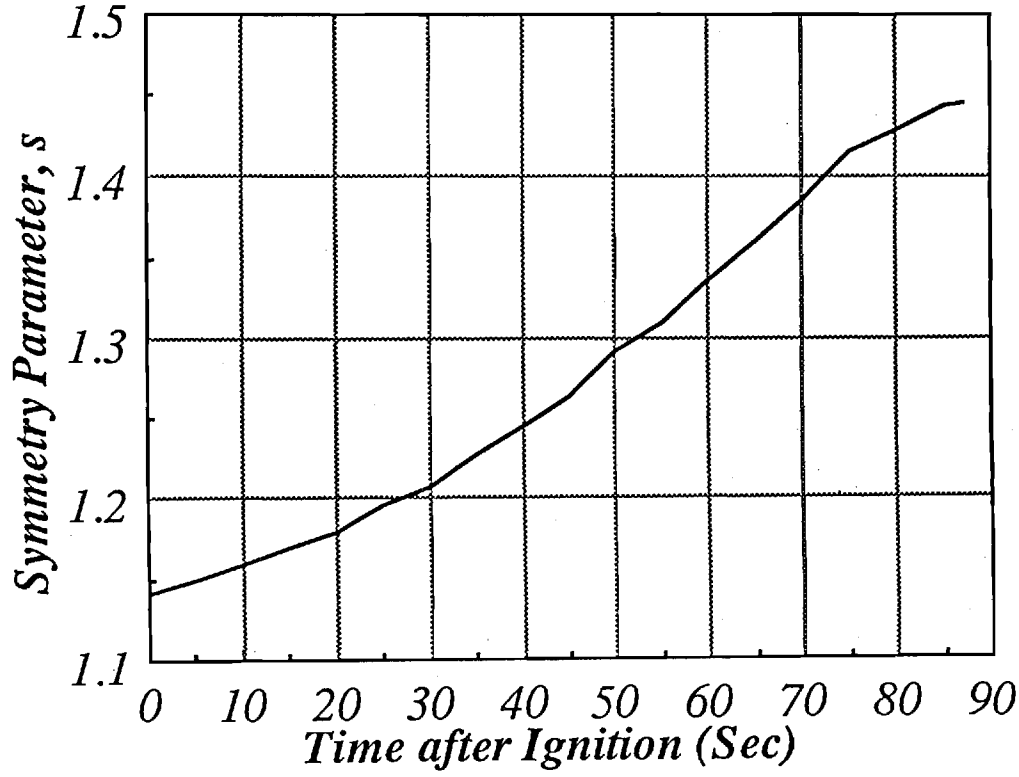

Figure 25. Symmetry Parameter s, Ulysses

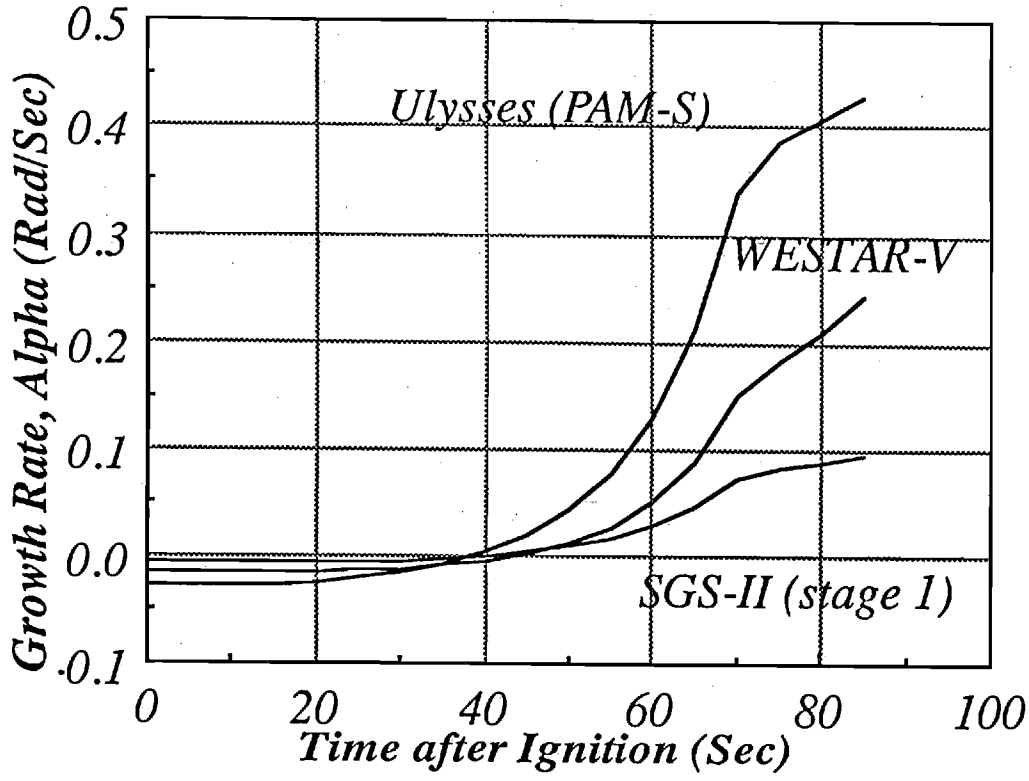

Figure 27. Comparison of Predicted Growth Rate

The actual nutation growth pattern is dependent on the initial wobbling present at motor ignition. It is also affected by presence of thrust offsets and by mid-burn transient effects described earlier. These lead to larger coning growth because they trigger the self-excited nutation oscillations. Thus, it is useful to first examine predicted motion in the absence of these triggering effects. Figure 28 is a plot of predicted nutation growth without sideforces using the predicted *Rgain* shown in Figure 24. The initial pitch angular velocity was assumed to be 0.2 degrees/second, which is typical of the PAM-D flights. Rapid divergence occurs during the last 10-15 seconds of the motor burn. On the scale of the plot the initial nutation oscillations are indiscernible. The very large predicted angular rate greater than 100 degrees/second corresponds to a final cone angle of about 50 degrees. It should be understood that this prediction is based on a linearized model for the gas flow interactions. Nonlinear effects would be brought into play long before such a large nutation angle is reached. These are expected to introduced additional damping such that smaller growth and a smaller final cone angle would result. The analysis assumes that the ratio of the lateral angular velocity is small compared to the spin angular rate. Thus the predicted motion beyond the 80 second point in Figure 28 where the lateral angular rate approaches about 25% of the spin angular rate is not reliable. Nevertheless, since vehicle stability is of primary concern, it is clear that a significant nutation problem exists in the Ulysses system if no attitude control is employed.

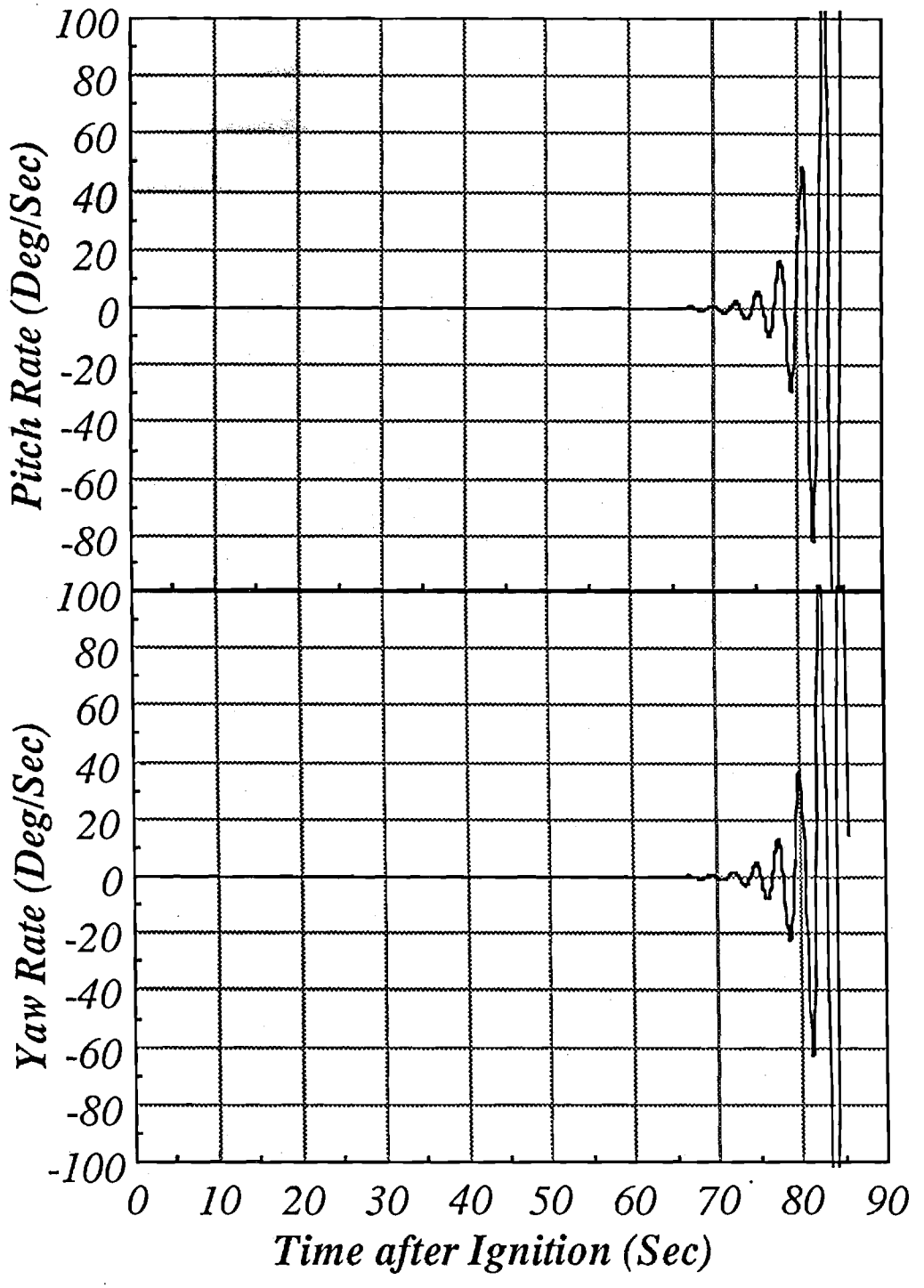

Figure 28. Ulysses - Predicted Nutation Rates with No Side Force.

To determine the effects of lateral forces due to CG or thrust offsets on the expected nutation growth, a typical measured side force time history was incorporated in the simulation computer program. Figures 29 and 30 show the assumed lateral force and its orientation relative to the spacecraft. These are based on data taken in STAR-48 static motor test Q-7. Figures 31and 32 show the effects of this lateral force pattern on the Ulysses vehicle in terms of the pitch and yaw angular velocities. Initial pitch angular rate was assumed to be 0.2 deg/sec. The only flow effect represented is the standard jet damping effect. Note that the main effect of the thrust offset is to displace the angular velocity plots. At burnout, the residual offset gives rise to nutation oscillations, which persist thereafter since there is no damping present. This effect is probably responsible for the unusual behavior at taildown that can be seen in the SGS rate plot (Figure 21). Lateral forces during the taildown process are unpredictable.

Figure33 shows plots of predicted nutation angular velocity for the Ulysses spacecraft with the Q-7 side loads, standard jet damping and the calculated Jet Gain effects. The latter so overwhelm the motion that the effects of the sideforce are difficult to see in the nutation rate plot in Figure 33. An initial pitch angular velocity of 0.2 deg/sec was assumed. As already discussed, the large values of lateral angular rate appearing in the last 10-15 seconds do not represent a reliable prediction of the actual motion, since nonlinear effects would be expected to dominate at rates approaching an appreciable percentage of the spin angular velocity.

The presence of the side force alters the system response to the Jet Gain effect by acting as a triggering mechanism. This is a potentially important aspect of the nutation instability problem that justifies further study, since there appears to be considerable uncertainty in the actual body-fixed side forces appearing in flight. The attitude control system must be capable of countering both the self-excited part of oscillations and the side force effects, since the latter can lead significant nutation oscillations in the post burn coast as already demonstrated. It is possible that in some cases a large part of the attitude control energy would be required to counter the thrust misalignment effects.

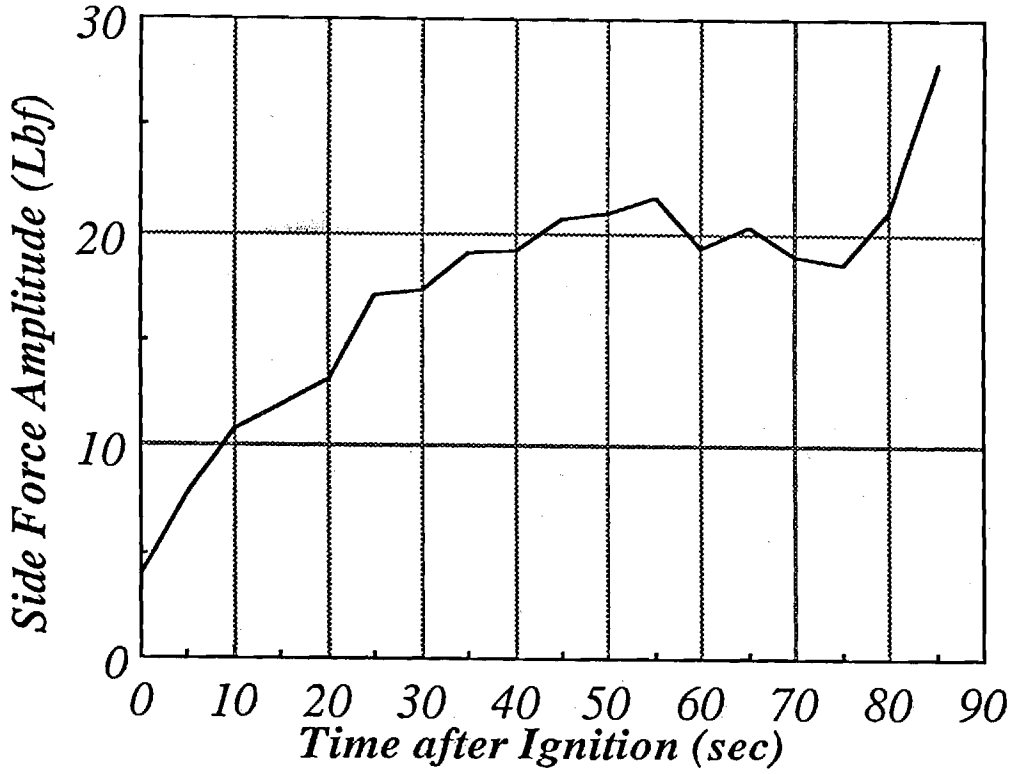

Figure 29. Side Force From STAR-48 Q-7 Static Test

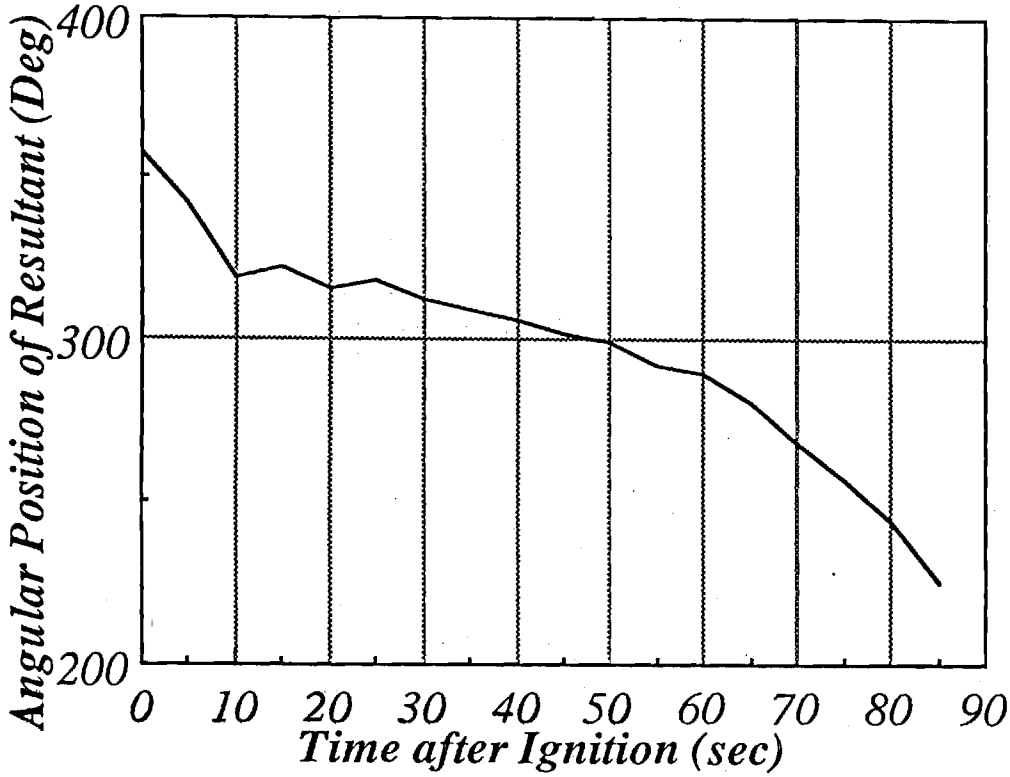

Figure 30. Side Force Orientation from STAR-48 Q-7 Static Test

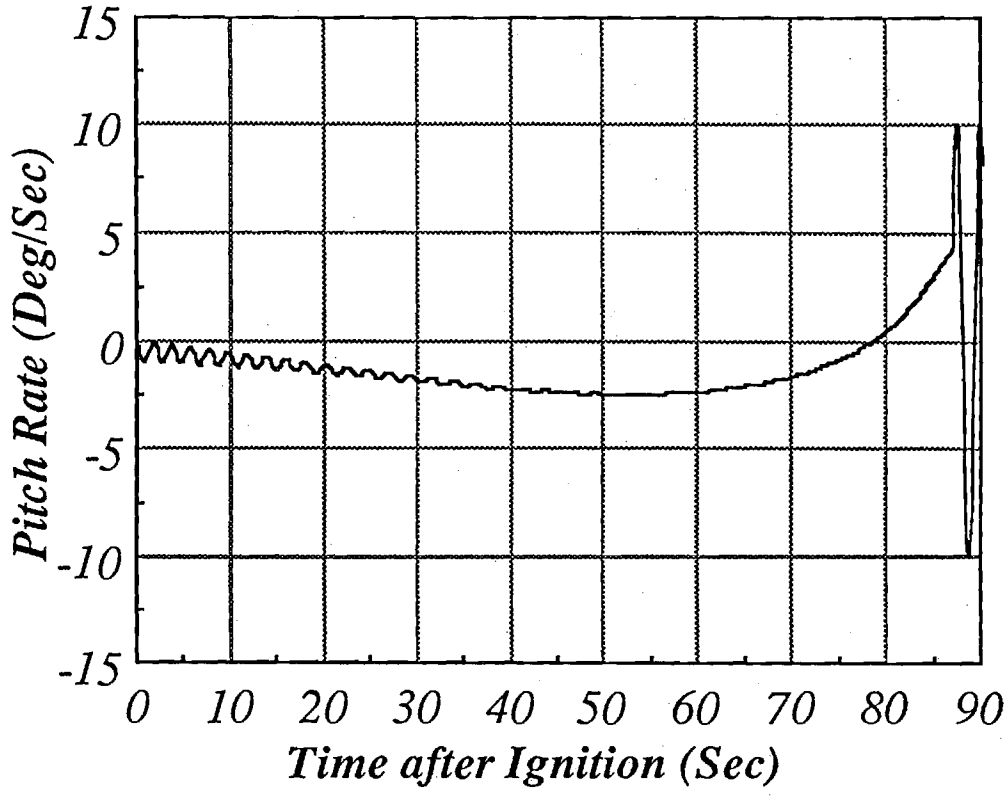

Figure 31. Ulysses - Predicted Pitch Rate with No Jet Gain & Q-7 Side Force.

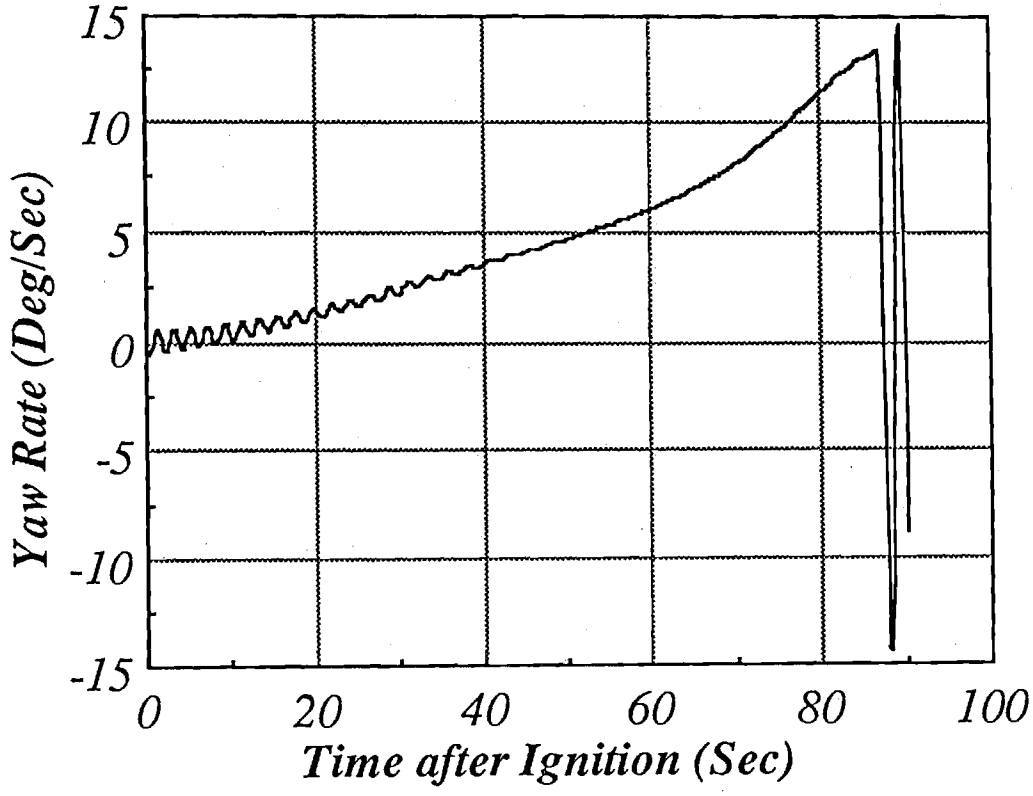

Figure 32. Ulysses - Predicted Yaw Rate with No Jet Gain & Q-7 Side Force.

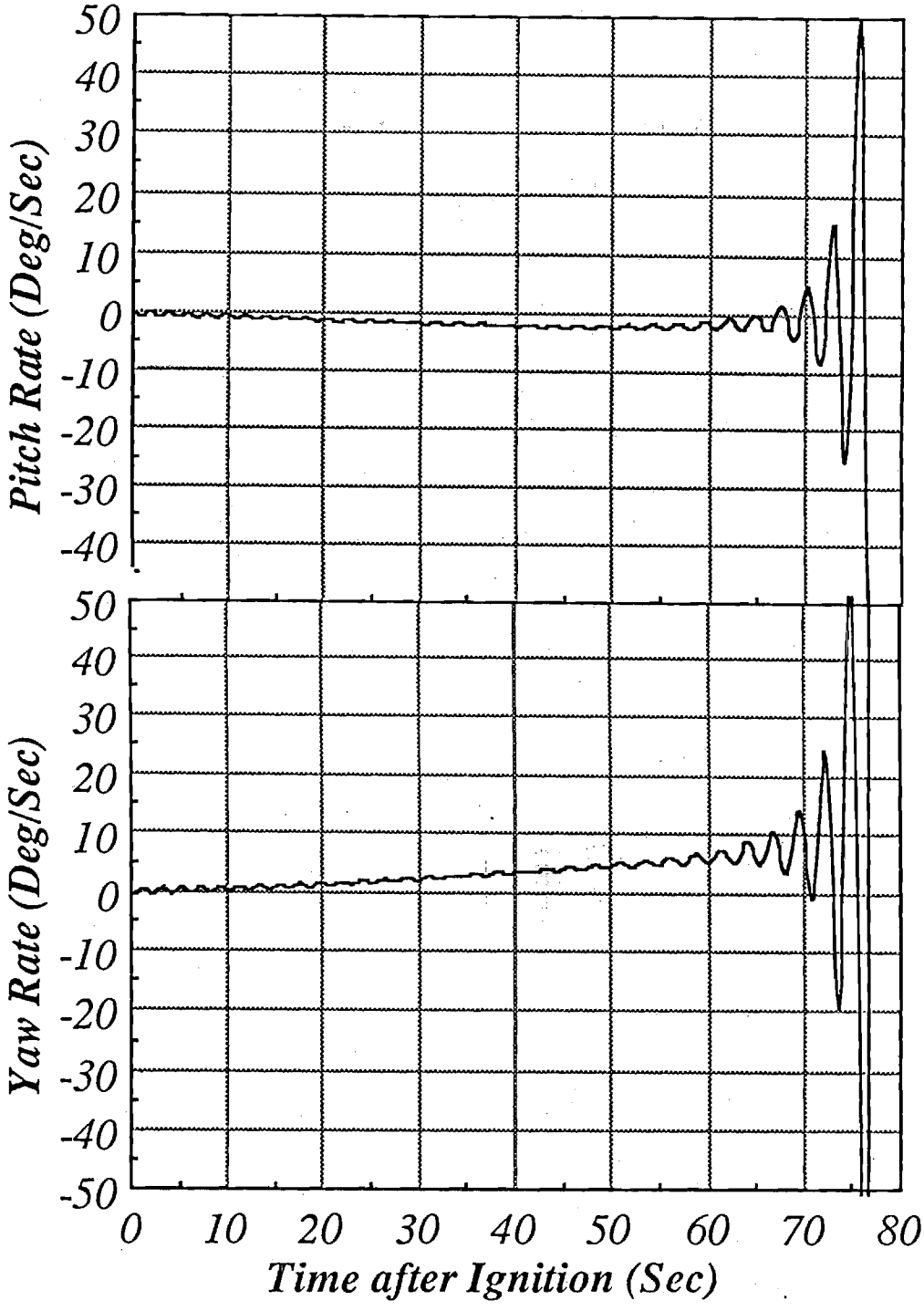

Figure33. Ulysses Predicted Nutation with Q-7 Sideforces

4.0 CONCLUSIONS

The results of this study indicate that the Ulysses spinning spacecraft design utilizing a standard STAR-48 rocket motor must incorporate attitude control capability if serious wobbling instability is to be avoided during motor operation. If no ACS is utilized, final cone angles greater than 55 degrees are predicted. The torque gains factors for the Ulysses system are similar in magnitude (maximum *Rgain* is roughly 4.5 ft-lbf/deg/sec) to those appearing in the PAM-D vehicles. Thus, relatively small attitude control torque capability is needed to control the self-excited nutation oscillations caused by interaction with the motor gas flow. A system similar in design to that used successfully in the SGS-II program should provide adequate control. Provision should be made to null the effects of thrust or center of mass offsets. These are readily detected both in accelerometer and rate gyroscope signals. A lightweight ACS system with the necessary capability can be designed using established techniques (see Reference 5). The body-fixed side force effects are likely to dominate the control system design. If the forces measured in the STAR-48 Q-7 test were to appear in flight, then a maximum control torque of about 100 ft-lbf. would be required to control nutation growth and vehicle attitude.

It is highly recommended that efforts be made to secure additional data regarding the nutation instability mechanism by means of full-scale static motor firings or flight tests. Tests in spinning compliant test stands could simulate flight conditions to the degree necessary to invoke the gas dynamic phenomenon on which the present analysis is based. Since slag accumulation in static test is expected to be much smaller than in flight, then such a test would either eliminate or verify the jet gain nutation mechanism. It is essential that the characteristics of the mechanism be fully understood in order that the design of reliable corrective attitude control devices can be properly matched to the vehicle configuration.

5.0 REFERENCES

1. Flandro, G. A., et al, "Fluid Mechanics of Spinning Rockets," AFRPL TR-86-072, Air Force Rocket Propulsion Laboratory, Edwards Air Force Base, January 1987.

2. Bolster, W., "Delta/PAM Coning," Internal Memorandum, NASA Goddard Spaceflight Center, Greenbelt, MD, July 1982.

3. McGarvey, J. F., "Delta/PAM Coning," (Attachment to memorandum by W. Bolster), NASA Goddard Spaceflight Center, Greenbelt, MD, 1982.

4. Walters, A. G., "Non-symmetric Flow in Laval Type Nozzles," Roy. Soc.Phil.Trans., A, Vol. 273, 185-235, 1972.

5. Webster, E. A., "Active Nutation Control for Spinning Solid Motor Upper Stages," AIAA 21st Joint Propulsion Conference, Monterey, CA, July 1985.